A framework for experimental determination of localised vertical pedestrian forces on full-scale structures using wireless attitude and heading reference systems

Journal of Sound and Vibration 376 (2016) 217–243

Contents lists available at ScienceDirect

Journal of Sound and Vibration

journal homepage: www.elsevier.com/locate/jsvi

A framework for experimental determination of localised vertical pedestrian forces on full-scale structures using wireless attitude and heading reference systems

M. Bocian [a,*], J.M.W. Brownjohn [b], V. Racic [c,d], D. Hester [e], A. Quattrone [f], R. Monnickendam [b]

[a] Department of Engineering, University of Leicester, University Road, LE1 7RH Leicester, UK
[b] Vibration Engineering Section, College of Engineering, Mathematics and Physical Sciences, University of Exeter, North Park Road, EX4 4QF Exeter, UK
[c] Department of Civil and Structural Engineering, University of Sheffield, Mappin Street, S1 3JD Sheffield, UK
[d] Department of Civil and Environmental Engineering, Politecnico di Milano, Piazza Leonardo da Vinci, 32, 20133 Milano, Italy
[e] School of Planning, Architecture and Civil Engineering, Queen's University Belfast, Stranmillis Road, BT9 5AG Belfast, Northern Ireland, UK
[f] Department of Structural and Geotechnical Engineering, Politecnico di Torino, 24 Corso Duca degli Abruzzi, 10129 Torino, Italy

ARTICLE INFO

Article history:
Received 21 August 2015
Received in revised form
2 May 2016
Accepted 3 May 2016
Handling Editor: J. Macdonald
Available online 16 May 2016

Keywords:
Loading from walking pedestrians
Force location tracking
Human–structure interaction
Wireless sensor network
Vibration serviceability of structures
Pedestrian dead reckoning

ABSTRACT

A major weakness among loading models for pedestrians walking on flexible structures proposed in recent years is the various uncorroborated assumptions made in their development. This applies to spatio-temporal characteristics of pedestrian loading and the nature of multi-object interactions. To alleviate this problem, a framework for the determination of localised pedestrian forces on full-scale structures is presented using a wireless attitude and heading reference systems (AHRS). An AHRS comprises a triad of tri-axial accelerometers, gyroscopes and magnetometers managed by a dedicated data processing unit, allowing motion in three-dimensional space to be reconstructed. A pedestrian loading model based on a single point inertial measurement from an AHRS is derived and shown to perform well against benchmark data collected on an instrumented treadmill. Unlike other models, the current model does not take any predefined form nor does it require any extrapolations as to the timing and amplitude of pedestrian loading. In order to assess correctly the influence of the moving pedestrian on behaviour of a structure, an algorithm for tracking the point of application of pedestrian force is developed based on data from a single AHRS attached to a foot. A set of controlled walking tests with a single pedestrian is conducted on a real footbridge for validation purposes. A remarkably good match between the measured and simulated bridge response is found, indeed confirming applicability of the proposed framework.

1. Introduction

Modelling the behaviour of lightweight structures due to the presence of active human occupants is a major challenge in the structural engineering community. The complexity arises owing to the highly adaptive nature of human behaviour and the potential of lightweight structures for dynamic response due to footfall loads, known as ground reaction forces (GRFs).

* Corresponding author. Tel.: +44 (0) 116 252 2539.
E-mail address: m.bocian@leicester.ac.uk (M. Bocian).

http://dx.doi.org/10.1016/j.jsv.2016.05.010
0022-460X/

Nomenclature

AHRS	altitude and heading reference system
BB	Baker Bridge
C7	seventh cervical vertebra
FEM	finite element model
GRF	ground reaction force
LB	lower back
LCS	local coordinate system
MCS	motion capture system
N	navel
oGRF	origin of the ground reaction force vector
PDR	pedestrian dead reckoning
QA	Honeywell accelerometer
S	sternum
TD	touch-down of the foot with the ground
TO	take-off of the foot from the ground
WCS	world coordinate system
ZUPT	zero velocity update

Both of these conditions can lead to human–structure interaction phenomena and emergent crowd behaviour, which might influence dynamic structural stability. Human–structure interaction refers to a feedback loop in which the energy is transferred between two dynamical systems – a human and a structure. Emergent crowd behaviour refers to the ability of a crowd to exhibit complex behaviours, resulting from simple local interactions between crowd members. Because of this complexity, the behaviour of an individual pedestrian must be first understood in order to build a reliable crowd–structure system model, including any relationships between the components of the system.

1.1. Background

Significant progress on this topic has been made in recent years by looking for inspiration in other fields of science, traditionally seen as unrelated to structural engineering. Physics-based, biomechanically-inspired modelling of pedestrian loading has revealed plausible mechanisms of pedestrian–structure interaction [1–5], some already supported by direct empirical evidence from laboratory investigations [6–8] and indirect evidence from measurements and modelling studies on full-scale structures [2]. Further progress is being made by turning attention to and drawing from achievements in the field of cognitive science. It is becoming evident that, in order to capture natural pedestrian behaviour, the experimental conditions during laboratory trials must closely resemble real life experience [8,9]. However, while this approach can help to understand adaptations in pedestrian gait invoked by the presence of structural motion, it does not provide any information about the behaviour of a pedestrian in a crowd. Resolution of this issue has been long overdue in the field of research concerned with the dynamic stability of structures.

Although increasingly sophisticated mathematical models of pedestrian–structure interaction and crowd dynamics appear regularly in scientific literature [10–12], most of them suffer from lack of hard evidence to support their main assumptions. This is particularly true for numerous models of synchronisation of walking pedestrians to structural motion or to each other, which are the most often purported mechanisms responsible for the build-up of large amplitude structural vibrations. This problem has persisted due to lack of suitable technology allowing pedestrians' and structural behaviour to be measured simultaneously in situ [13]. As a result, loading models are usually derived and extrapolated to real life structures based on laboratory test data, most often collected while walking on a rigid surface in an environment offering incongruent sensory information and preventing a test subject to freely adjust their gait. These limitations can be argued to be the root cause of instability of the London Millennium Footbridge [14].

To address the abovementioned limitations of current modelling approaches a few attempts have been made in recent years to develop a suitable framework for capturing pedestrian behaviour in situ. Two main technology trajectories are being explored – optical motion capture systems (MCS) and wireless inertial measurement units or monitors. These monitors, when using a fusion algorithm to compute global orientation (i.e. relative to the direction of gravity and Earth's magnetic field) from a triad of accelerometers, gyroscopes and magnetometers along with motion data, are referred to as Attitude and Heading Reference Systems (AHRS), and a single monitor is *an* AHRS. An optical MCS, managed by a dedicated data processing unit, consists of cameras tracking coordinates of markers.

1.2. Recent advances in in-situ measurement of pedestrian forces

The applicability of wireless AHRS for characterisating pedestrian walking forces was studied by Van Nimmen et al. [15]. In their modelling framework acceleration data from an inertial monitor attached at pedestrian waist level were used to obtain information on timing of footsteps. Subsequently, the loading model proposed by Li et al. [16] was fitted for the duration of each single step. This model relies on summing five Fourier components representative of mean pacing frequency and its higher harmonics, with amplitudes scaled in proportion to the walker body mass. Although the approach (i.e. attempting in-situ measurement of pedestrian forces on a real structure) is an advance on earlier work in the area, some limitations remain. For example, assigning a simple load shape function based on Fourier decomposition, even if implemented when footstep onset is not periodic, introduces certain artificial repeatability and neglects genuine time and amplitude variability present in force patterns, some of which can be associated with human–structure interaction. Some

concerns were acknowledged by the authors of [15] during a discussion of findings from a series of controlled loading tests where up to six pedestrians walked on a full-scale footbridge. It was noted that, for the single record of vertical response presented, when the reconstructed force from four pedestrians (calculated using the proposed load modelling framework) was applied to a numerical model of the bridge, the vertical response levels were three times those measured. While there was some uncertainty about the modal characteristics of the footbridge used for the test, the main source of discrepancy was assigned to human behaviour and shortcomings of the adopted loading model [16]. Another possible source of simulation error is that walker position was inferred using an assumed constant walking velocity, calculated from bridge length and test duration. Accurately knowing the position of the walker is important as the modal force estimation requires the instantaneous amplitude of pedestrian loading to be modulated by the localised mode shape amplitude.

More recently recommendations have been made by Dang and Živanović [17] as to a marker model for reconstructing pedestrian vertical force using an inverse dynamics procedure [18] based on data collected from an optical MCS in laboratory conditions. In short, this procedure relies on division of the human body into a number of interconnected segments of known length and position. The mass and position of the centre of mass is then determined for each segment based on anthropometric data, allowing the motion of the centre of mass (CoM) of the whole body to be calculated, from which the force is obtained in line with Newton's second law of motion. Dang and Živanović [17] found that, for stamping on a spot on a force plate, a model consisting of 19 markers was able to yield an absolute error in the amplitude of the component of force at the fundamental stamping frequency, against the directly measured force, of up to 15 percent in 90 percent of the trials. Additional tests were conducted during which a subject walked on a treadmill placed at the midspan of a flexible bridge. The absolute error in the average peak-per-cycle bridge response acceleration reconstructed based on the model, against the measured response, was up to 20 percent in 92 percent of the trials.

There are several practical drawbacks in using an optical MCS for measuring pedestrian kinematic data outdoors for pedestrian force reconstruction. Covering the volume of interest, e.g. the whole length of a footbridge, requires many cameras, at considerable economic and time cost [19,20]. Marker occlusion from fellow occupants of the structure and features of the environment is also a problem since, for optimal performance, all markers need to remain visible to at least two cameras at all times. Lighting conditions are a major problem, especially cloud cover alternating with strong sunlight, and operation of systems using active infrared light can be seriously compromised by fictitious data resulting from infrared components of solar radiation. Because of these limitations and due to growth in technology for personal instrumentation, for field work, a system using AHRS is advantageous.

1.3. The scope of this study

The goal of this study is to develop a framework for determining the localised vertical component of GRF on a structure in-situ while avoiding any rebuttable presumptions of the pedestrian behaviour. This could provide the means to calibrate both deterministic and stochastic models of GRFs of individuals and crowds along with structural response, and to investigate the interaction phenomena pertaining to the crowd–structure system, which could be critical for dynamic structural stability. Wireless AHRS were chosen due to practical advantages in system deployment, compact size and ease of use in the field.

The rest of the paper is organised as follows. Section 2 presents a study conducted to corroborate a pedestrian vertical force model based on a single point inertial measurement acquired with an AHRS. A pedestrian dead reckoning algorithm used to reconstruct the instantaneous position of pedestrian's foot based on data from a foot-mounted AHRS is then described in Section 3. Another algorithm is proposed in Section 3, which allows origin of the GRF vector (oGRF) to be located. Section 4 is concerned with a controlled pedestrian loading test performed on a 109 m long cable stayed footbridge to gather data allowing the proposed modelling framework to be validated. A study aiming at verifying the response obtained using the proposed framework against the measured responses is presented in Section 5. Concluding remarks are presented in Section 6.

2. Pedestrian loading model based on a single point inertial measurement

The first step in formulating the proposed framework was to evaluate whether a single point inertial measurement could be used to reproduce pedestrian vertical force in enough detail for it to be suitable for use in structural loading models. With this aim in mind, a dedicated experimental campaign was conducted during which test subjects instrumented with AHRS and also monitored with an optical MCS performed walking tests on an instrumented treadmill located in the Light Structures Laboratory of the University of Sheffield, UK. The data obtained from the treadmill were used to benchmark the loading model. The study was approved by the University of Sheffield Research Ethics Committee.

2.1. Overview of the experiments

Six subjects (S1–S6), all healthy British male adults in their early twenties, participated in the study. Their basic anthropometric data are given in Table 1. All subjects had prior experience with walking on a motorised treadmill, all signed an informed consent form and all completed a physical activity readiness questionnaire.

Each subject wore gym-type shoes and tight-fitting gym clothes allowing AHRS to be placed at four specific locations on their body, namely seventh cervical vertebra (neck), sternum, navel and fifth lumbar vertebra (lower back), as can be seen in Fig. 1. At least 8 min of habituation to the experience of walking on the treadmill in the laboratory environment was given to each subject. Each subject then participated in six walking tests in which the imposed speed of treadmill belts was typically between 0.6 and 1.4 m s^{-1}. The choice of the speed was determined by first allowing the subject to establish a comfortable speed, and then varying the speed in approximately 10 percent increments, such that there was one speed faster than comfortable and four speeds slower. While speeds faster than 1.4 m s^{-1} have been observed among pedestrians walking on real structures [21], this upper speed limit was imposed for experimental protocol to comply with the requirements of the University of Sheffield Research Ethics Committee, to prevent tests subjects from discomfort. Each test lasted for approximately three minutes, which, after discarding periods associated with gait and instrumentation initiation and termination stages, allowed approximately two minutes of data to be obtained for further processing. To prevent bias due to subject's predictive behaviour and account for the change of behaviour with time e.g. due to fatigue, the order of tests was randomised.

2.2. Instrumentation

Three independent instrumentation systems were deployed during the experiments – an ADAL3D-F split-belt instrumented treadmill [22], wireless APDM Opal™ monitors [23] and Codamotion optical MCS [24]. The analyses presented in this section are based on data from the former two systems only and their relevant specifications are given in more detail. The MCS mainly functioned as a data acquisition system, simultaneously recording force data from the treadmill and triggers generated by the wireless system in the form of sharp voltage spikes, allowing the beginning and end points of their signals to be identified within treadmill data.

2.2.1. Instrumented treadmill

The vertical forces exerted by a pedestrian on the walking surface were measured directly by the ADAL3D-F which incorporates a force plate under each of the two parallel treadmill belts. Built specifically for clinical gait analysis, the treadmill is stiff enough not to cause pollution of the measured signals with errors due to resonance and flexure. The data from the treadmill calibrated to engineering units of force were acquired via proprietary software at a rate of 1 kHz.

2.2.2. Wireless AHRS

Six APDM Opal™ AHRS and a wireless access point allowed real-time wireless data streaming and communication with a host computer. Each AHRS (or *monitor*), based on Micro-Electro-Mechanical System (MEMS) technology, incorporates

Table 1
Basic data for all experimental subjects for tests conducted on an instrumented treadmill.

Subject ID	S1	S2	S3	S4	S5	S6
Mass m_p [kg]	90	75	81	60	93	64
Height h [m]	1.83	1.80	1.90	1.79	1.88	1.74
Age [years]	21	22	21	22	21	21

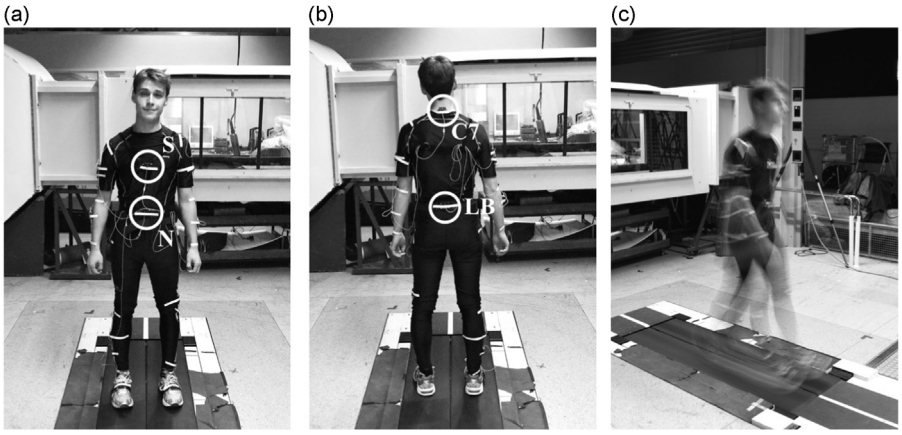

Fig. 1. (a) Opal™ AHRS monitors attached at the sternum (S) and navel (N) levels (b) Opal™ AHRS attached at the fifth lumbar vertebra (lower back; LB) and seventh cervical vertebra (neck; C7). (c) A subject during a walking test on a split-belt instrumented treadmill.

triaxial magnetometer sensing orientation against the direction of a magnetic field, triaxial accelerometer, and a triaxial gyroscope sensing rate of change of rotation, and a temperature sensor. In order to recover motion in three-dimensional space, the sensors axes form a right handed triad. AHRS resources are managed by a microcontroller and wireless communication is achieved with a radio module. In the laboratory treadmill tests monitor data were streamed wirelessly to a host computer, although each monitor also contains on-board flash memory allowing direct logging, a feature used during tests on a full-scale structure reported in Section 5. Opal™ monitors are different from *inertial measurement units* which provide data on translational and rotational movements only. This is because Opals™ incorporate a magnetometer, which allows their orientation to be determined relative to the Earth's gravity and magnetic field [25].

Proprietary software of APDM (Motion Studio, version 1.0.0.2015) was used for system calibration and data retrieval. All monitor data were sampled at 128 Hz and, since the force amplitude for the chosen conditions was not expected to exceed twice body weight, accelerometer operational ranges were set to 2 g.

2.3. Data processing

The main goals of data processing were to derive a pedestrian vertical loading model based on AHRS data and to benchmark this model against the vertical component of pedestrian GRF measured from the treadmill. This section describes procedures adopted in order to realise these goals and establishes quality indicators for evaluation of the proposed pedestrian loading model.

2.3.1. Treadmill data

After correcting for the drift associated with piezoelectric effect exploited by the force transducers, calibrated treadmill data were aligned with AHRS data using triggers recorded by the wireless system (see Section 2.2). All data were set to a common sampling rate of 128 Hz. A delay-compensated antialiasing finite impulse response low-pass filter was used in down-sampling data from the treadmill. Exemplar calibrated force traces from the right and left leg corrected for drift are shown in Fig. 2. All data are unfiltered and for S2 walking at 1.28 m s^{-1}. Take-off (TO) and touch-down (TD) events at which the foot loses and regains contact with the ground, respectively, were detected in the drift-corrected data. This was necessary because reliable estimates of pedestrian force amplitudes in spectral calculations require that the analysed record should contain an integer number of pedestrian walking cycles. A force threshold of 10 N was chosen for these analyses. An exemplar application of this threshold for detection of TD (circles) and TO (dots) is shown in Fig. 2, for S2 walking at 1.28 m s^{-1}.

2.3.2. AHRS data used in the pedestrian vertical loading model

An underlying assumption in deriving a loading model based on a single point inertial measurement is that the recorded motion of the monitor represents the motion of the CoM of the whole body. A similar approach, albeit based on MCS data, was previously used in an attempt to reconstruct the lateral component of pedestrian force on laterally-oscillating ground [26], and human jumping forces [27]. The pedestrian force can be obtained directly by applying Newton's second law of motion:

$$F(t) = \underbrace{m_p g}_{\text{staticforce}} + \underbrace{m_p a_M(t)}_{\text{dynamicforce}} \tag{1}$$

where m_p is the pedestrian mass, g is gravitational acceleration and a_M is the acceleration measured by a monitor. This assumption is substantiated for acceleration data from a monitor attached at waist level since, although not directly linked to any anatomical body landmarks, the CoM excursions in walking can be expected to fluctuate around the superior aperture

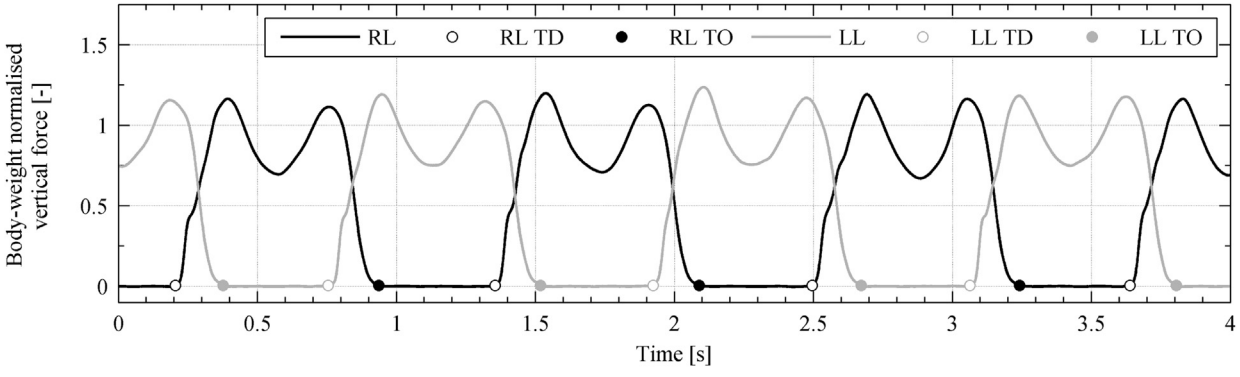

Fig. 2. Exemplar body weight-normalised vertical pedestrian force from treadmill for right and left leg (RL and LL, respectively). Also denoted on the plot are touch-down (TD) and take-off (TO) events for both legs.

of the pelvis [28]. However this cannot be assumed to be true for other monitor locations. Nevertheless, performance of this simple loading model was tested on data from monitors attached at four different locations on the subject's body: the fifth lumbar vertebra (lower back), navel, sternum and the seventh cervical vertebra (C7; neck), which are shown in Fig. 1. Elastic straps were used to secure all monitors except when placed on C7 where the monitor was secured with medical-grade double-sided tape. The locations as well as the loading models that use monitors at these locations are referred to here as LB, N, S and C7, respectively.

For the loading model to be applicable it must provide the pedestrian force in a reference frame meaningful from the structural standpoint, yet each monitor senses acceleration in its local (i.e. monitor) coordinate system (LCS). Despite the most careful monitor placement, its orientation is bound to change while walking, hence alignment of one monitor axis with the vertical direction in world (i.e. Earth) coordinate system (WCS) cannot be guaranteed and must be resolved from LCS data. For each data set associated with a single time stamp, each monitor encodes a four-dimensional complex number, known as quaternion, representing monitor orientation against a magnetic North, West and vertical-up Earth reference frame. The data in LCS were transformed to WCS using quaternion algebra [29].

2.3.3. Evaluating the pedestrian vertical loading model

For structural vibration serviceability, the most important component of pedestrian vertical force is at the fundamental walking frequency, hence evaluation of the pedestrian loading model presented in this paper mostly focuses on this force component. The evaluation of the data from the loading models is carried out in Sections 2.4 and 2.5 while the theory behind the evaluation process is briefly described below.

The proposed loading model assumes that monitor data represent motion of the CoM (see Section 2.3.2) hence the force reconstructed with Eq. (1) is the total pedestrian force. The corresponding total pedestrian force from the treadmill was obtained by summing the force signals from both treadmill force plates (see Fig. 2), and the amplitude of the force component of interest was extracted from the Fourier magnitude of force obtained using the procedure outlined in Section 2.3.1.

In order to assess temporal congruence of the model with data obtained directly from the treadmill, Fourier semblance was calculated [30]:

$$S_{T,M}(f)=\frac{\Re_T(f)\Re_M(f)+\Im_T(f)\Im_M(f)}{\left[\Re_T^2(f)+\Im_T^2(f)\right]^{0.5}\times\left[\Re_M^2(f)+\Im_M^2(f)\right]^{0.5}} \tag{2}$$

where f is the frequency, $S_{T,M}$ is the semblance between the force from the treadmill (denoted by subscript T) and the force reconstructed based on Opal™ acceleration data (denoted by subscript M), and $\Re$ and $\Im$ denote the real and imaginary part of the complex Fourier coefficient. This approach is more intuitive than simply stating phase difference in an angular scale since, similarly to the Pearson's correlation coefficient, Eq. (2) returns values from -1 to $+1$, where -1 and $+1$ imply perfect out-of-phase and in phase correlation, respectively, and 0 implies lack of correlation.

Performance of the loading model derived from Eq. (1) was assessed in statistical terms by estimating empirical cumulative distribution functions. Absolute percentage error value in the amplitude of pedestrian vertical force component at the fundamental walking frequency reconstructed based on Opals™ acceleration data, ΔF, was used as a quality indicator. It was calculated according to

$$\Delta F=\left|\frac{F_T-F_M}{F_T}\right|\times 100\% \tag{3}$$

where F_T and F_M are the amplitudes of Fourier force components at the fundamental walking frequency obtained from data from the treadmill and Opal™ monitor, respectively.

2.4. Results and discussion

Results from analysis of data collected from the experimental campaign are reported in this section. The data presented in Section 2.4.1 relate to S2 ($m_p=75$ kg and $h=1.8$ m) walking at 1.28 m s^{-1}. The choice of this particular dataset was dictated by several factors. First, the walking velocity is close to the average walking velocity measured on some footbridges (1.3 m s^{-1}) [21]. Second, the subject's mass and height are close to the average values for the male English population aged 16–24 (74.8 kg and 1.776 m) [31]. Nevertheless, the relationships discovered in the data apply for all participants of the campaign.

2.4.1. Amplitude and timing

Exemplar truncated time histories of body-weight normalised vertical force measured directly by the treadmill and reconstructed based on Eq. (1) are presented in Fig. 3. Footbridge vibration serviceability assessments rarely consider more than the first or second harmonics of pacing rate. However, to allow a more detailed comparison between the forces measured by the treadmill and the forces predicted by the loading model, a two-way second-order Butterworth low-pass filter with cut-off frequency 8 Hz was applied to all the data. Part (a) of Fig. 3 shows the force calculated from a monitor attached at the lower back (LB) and navel (N), whereas part (b) shows the force calculated from a monitor attached at the sternum (S) and neck (C7).

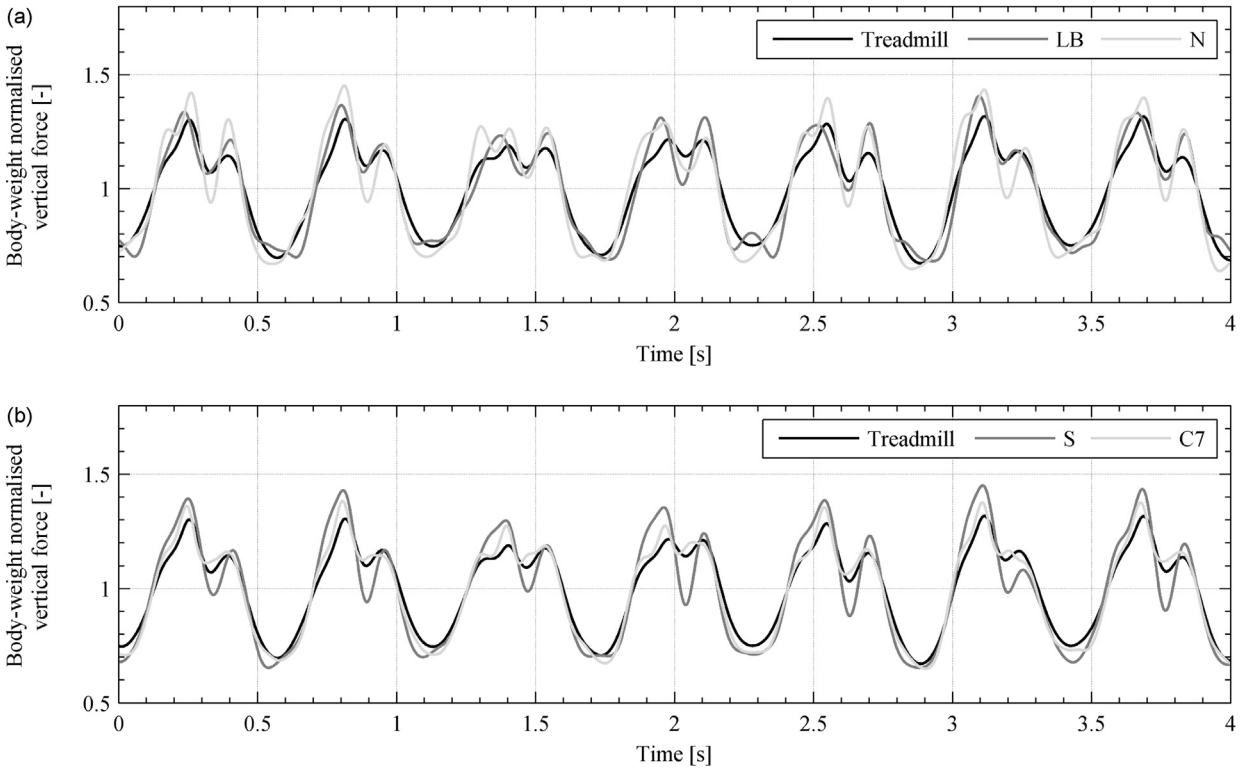

Fig. 3. Truncated time histories of pedestrian total vertical walking force from direct measurement (treadmill) and reconstructed based on acceleration acquired by monitors placed at (a) LB and N and (b) S and C7.

Visual inspection reveals that the patterns of variation of the reconstructed forces (calculated from the monitor data) resemble the characteristics of the force obtained from the treadmill, both in amplitude and shape. A remarkably good match can be seen for model C7 and the worst match for model N. Variability in the force amplitude is particularly pronounced for model S, indicating the presence of considerable energy at higher frequency components.

Single-sided power-preserving FFT magnitudes of data in Fig. 3, relieved of the static (0 Hz) force component and taken over a longer interval, are presented in Fig. 4. It can be seen in Fig. 4(a) and (b) that the proposed loading model can capture (at least qualitatively) all components of pedestrian vertical force, including those at $nf_p \pm 0.5f_p$, where f_p is the pacing frequency and n is a positive integer, which are most likely associated with gait laterality [9]. Good agreement between the directly measured force and the force reconstructed from the model around f_p is visible in Fig. 4(c) and (d). The spread of energy into neighbouring force components is caused by adaptations in gait pattern throughout the test. In most of the cases the accuracy of the loading model degrades for higher harmonics, most strongly for model S. In contrast, Fourier amplitudes of force from model C7 give a remarkably good match with the amplitudes of force measured directly on the treadmill, up to the fourth harmonic.

The overestimation of energy at higher frequencies is associated with noise in the kinematic data. This noise can arise due to soft tissue artefacts, slippage of the straps attaching monitors to subjects' bodies or interference of the monitor with underlying clothing. Better signal-to-noise ratio might explain why model C7, based on acceleration from a monitor attached directly to the skin with double-sided tape at the level of the seventh cervical vertebra, consistently outperformed other models.

The results of the analysis of data in Fig. 4 for temporal similarity are presented in Fig. 5. Reliable estimates of Fourier semblance are available for the components of force carrying significant spectral energy. The most important of these components are at nf_p, where n is a positive integer. The corresponding values of Fourier semblance are denoted by dots in Fig. 5.

In all cases time correlation in the component of force at the walking frequency obtained from the model and the treadmill is almost perfect, but can diminish for higher harmonics. The best temporal congruence can be seen for models S and C7. The aggregated measures of time correlation for the component of force at the fundamental walking frequency, for all of the conducted tests from a model associated with each monitor location, are given in Table 2.

The time correlation between the models and the treadmill data is generally strong, with mean Fourier semblance above 0.97 and mean standard deviation up to 0.032. Directionality of this relationship is indicated by the sign of mean phase difference. Model LB tends to lag data from the treadmill, but the opposite is observed for all other models. Standard deviation of phase difference is generally similar.

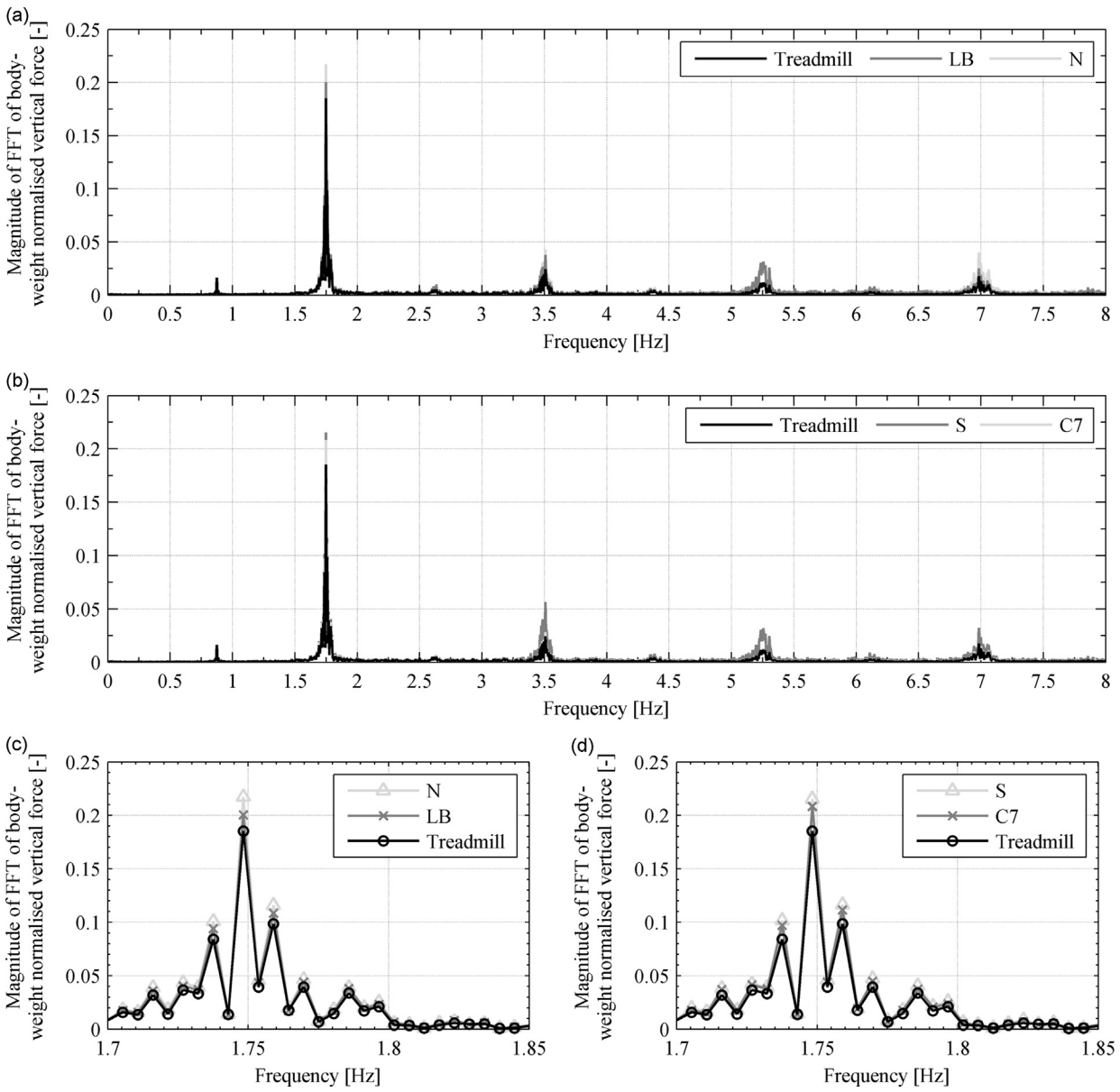

Fig. 4. Single-sided power-preserving magnitude of FFT of body-weight normalised vertical force from direct measurement (treadmill) and reconstructed based on data from monitors placed at (a) LB and N and (b) S and C7. The amplitudes of force components around the fundamental walking frequency are shown in more detail in (c) and (d).

2.4.2. The influence of walking velocity

The influence of walking velocity on the error in the predicted amplitude of the component of force at the walking frequency is shown in Fig. 6. Each plot contains data from all subjects (denoted by different symbols) from all of the conducted tests, from a model associated with one monitor location. Since the data in each plot show distinct ranges containing their minima and maxima, a best fit second-order polynomial is denoted on each plot as a black curve to show the data trend. To show significance of data scatter, 90 percent pointwise confidence bounds for a new observation are denoted in grey.

Models N and S most often overestimate the measured force and their patterns of variation of the error are similar, with the best fit curve in Fig. 6(b) for model N being almost linear within the range of the presented data. Therefore this model can be used to obtain conservative estimates of pedestrian force in vicinity of the fundamental walking frequency. Model N, for which the spread of data around the fit is less than for model S, yields an average absolute error of 11 percent. Taking all the above into account it is conceivable that model N, simply corrected for the offset by subtracting a constant, could be used to obtain reasonable estimates of pedestrian force for different walking velocities. Model LB performs well for normal

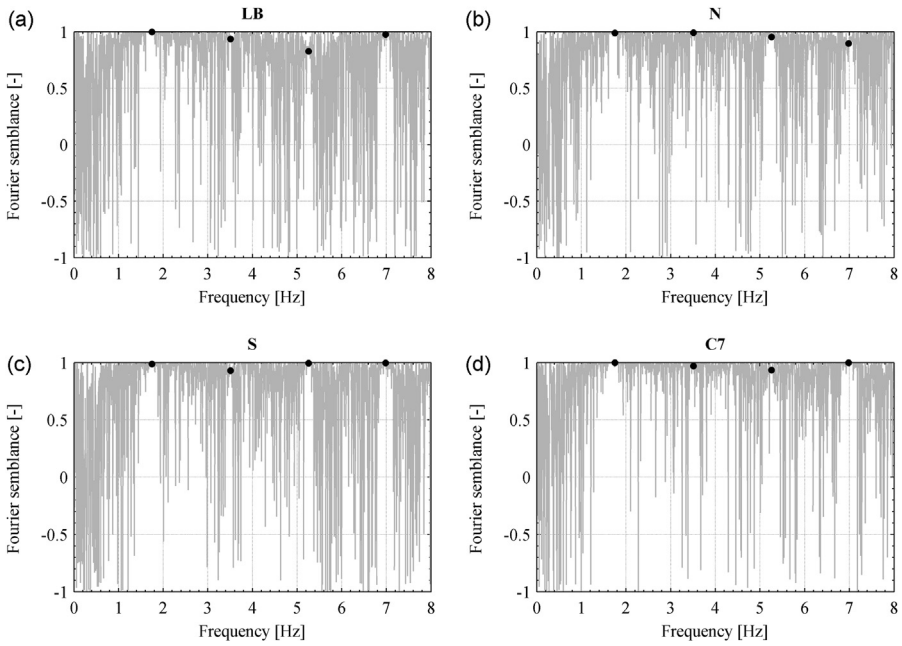

Fig. 5. Fourier semblance between the force from direct measurement and reconstructed based on data from monitors placed at (a) LB, (b) N, (c) S and (d) C7. Black dots denote the values corresponding to the component of force at the fundamental walking frequency and its harmonics.

Table 2
Mean Fourier semblance and phase difference for the component of force at the fundamental walking frequency based on data reconstructed with the model and measured directly on the treadmill. Values of standard deviation are given in brackets.

Model	LB	N	S	C7
Fourier semblance [n/a]	0.986 (0.024)	0.977 (0.028)	0.973 (0.032)	0.987 (0.022)
Phase difference [rad]	−0.022 (0.170)	0.161 (0.144)	0.182 (0.151)	0.076 (0.149)

walking speeds (i.e. above 1.2 m s^{-1}) yielding an average absolute error of 8 percent and maximum error of 15 percent. However, it suffers from increasing inaccuracies with decreasing walking speeds, both in terms of the mean error and its variability. A considerable dispersion of data for model LB might be associated with flexing back extensor (*erector spinae*) and surrounding muscles during the gait cycle. The strength of this effect is likely to be influenced by physiological composition of the tissue underlying the monitor and attaching straps.

The best agreement with the directly measured force is found for model C7, yielding average absolute error of 7.7 percent. However, Fig. 6(d) shows that the data from that model also lend themselves to a curvilinear fit. The reliability of the pedestrian loading models derived from Eq. (1) is further discussed in Section 2.5.

Subject-dependent trends can be identified in the data, for example, all data for S1, S3 and S4 lie below the fit in Fig. 6(a), while all data for the other subjects lie above that fit. Interestingly, similar subject-dependant trends in the error of force amplitude can be observed in data reported in [17]. Since this effect appears to be systematic, it is most likely caused by different body mass distribution of test subjects and inaccuracies in monitor (or marker) placement. This can distort the estimated motion of the CoM representing overall body dynamics, used for reconstructing pedestrian vertical force in both studies.

2.4.3. The influence of pacing frequency

It is well known that pacing frequency and walking velocity have a strong correlation [32] so it is no surprise that plots of error in fundamental Fourier amplitude component of vertical force against the pacing frequency (Fig. 7) show patterns resembling those errors plotted against walking speed (Fig. 6). Furthermore, as in Fig. 6, subject-dependent trends are visible in Fig. 7.

2.5. Reliability of the pedestrian loading model

Rather than fitting a certain distribution to data and analytically evaluating confidence levels, reliability of the loading models was assessed by inspecting the empirical (non-parametric) cumulative distribution functions. Error in amplitude of

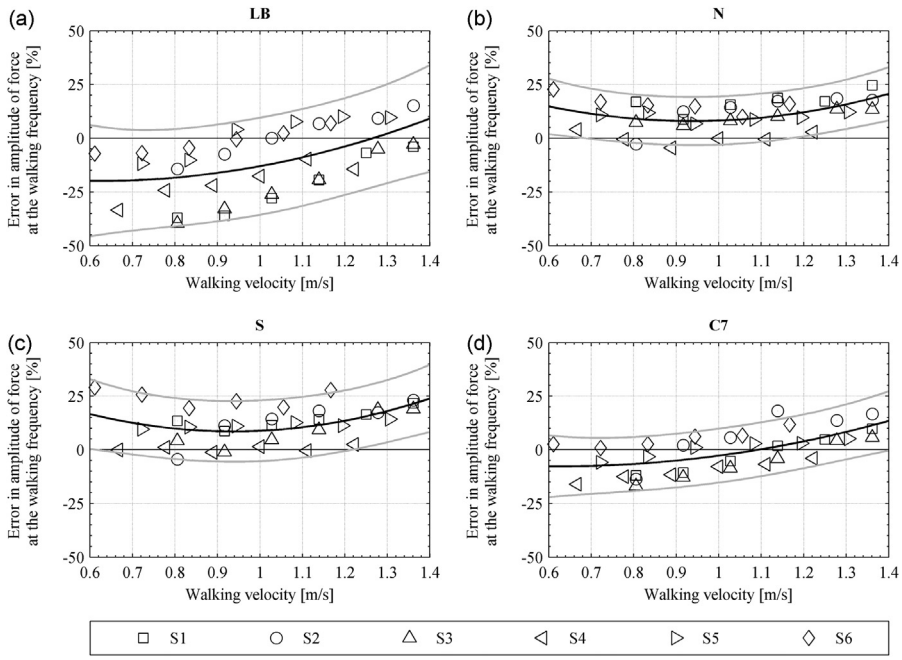

Fig. 6. Percentage error in Fourier force amplitude at fundamental walking frequency against walking velocity, for all subjects and tests, for data from (a) LB, (b) N, (c) S and (d) C7. The best fit second-order polynomial is also denoted on each plot as a black curve to show trends in the data, together with 90 percent pointwise confidence bounds denoted as grey curves.

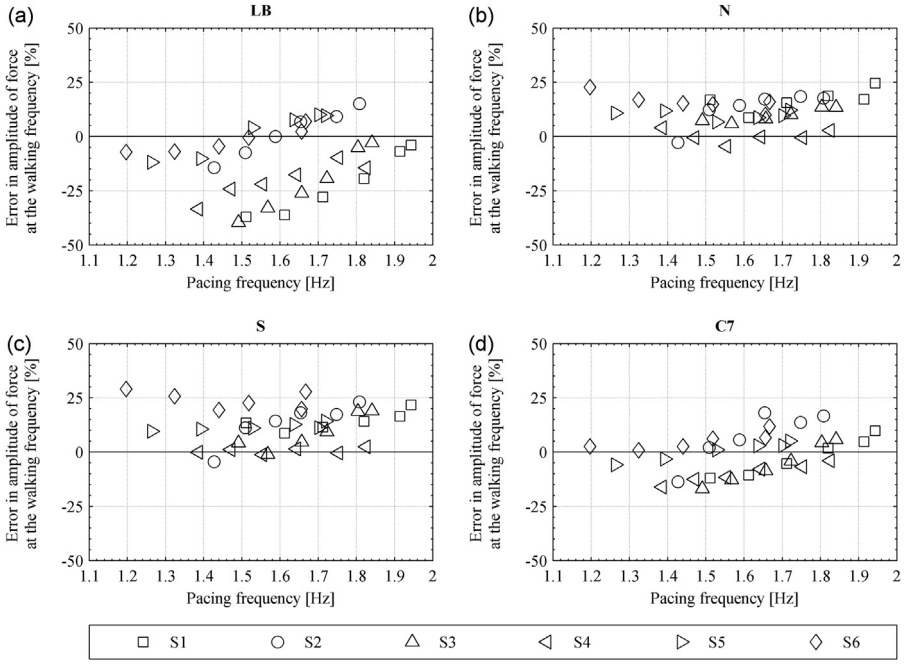

Fig. 7. The percentage error in Fourier force amplitude at the pacing frequency against that frequency, for all subjects and tests, for data from monitors placed at (a) LB, (b) N, (c) S and (d) C7.

the reconstructed force component at the fundamental walking frequency was used as a quality indicator (see Section 2.3.3). The same methodology was adopted in [17]. The results of this assessment are presented in Fig. 8.

Model C7 captures pedestrian loading relatively well, being able to achieve an absolute error below 15 percent at 90 percent probability of occurrence. Conversely, diminishing gradient of the cumulative distribution function for model LB indicates multiple outliers in the data, which correspond to lower walking speeds. Consequently, the overall performance of this model is relatively poor. Models N and S yield absolute errors below 18 percent and 23 percent, respectively, at 90

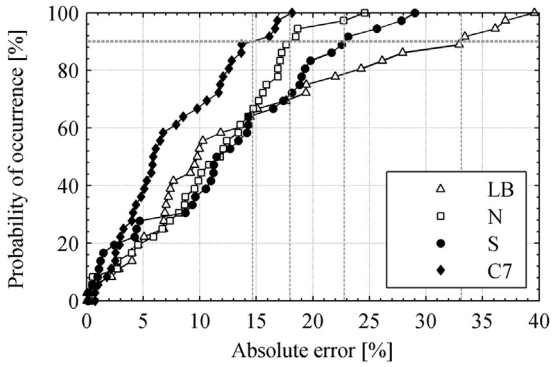

Fig. 8. Empirical cumulative distribution functions for absolute percentage error value in the amplitude of pedestrian vertical force component at the pacing frequency, reconstructed based on data from LB, N, S and C7. The values of the error corresponding to 90 percent probability of occurrence are indicated via grey lines.

percent probability of occurrence. Note that a fixed treadmill was used in validating the models, but it is assumed with supporting evidence [33], that a compliant structure does not significantly affect this validation.

Considering the simplicity of the proposed model and the consistency in the relationships discovered in the experimental data, it can be concluded that pedestrian vertical force model based on a single point inertial measurement can capture the characteristics of walking forces with a quantified good accuracy. To obtain the most reliable estimates of pedestrian vertical force at different walking speeds, model C7 is recommended. Considering the results reported in [26,27], it can be concluded that model C7 is the best for monitoring human body kinetics for a range of activities. For walking at a comfortable speed (above 1.2 m s^{-1}) model LB can also be used, if only the components of force at and around the first harmonic are considered. Model N could be used directly to obtain conservative estimates of pedestrian force around the fundamental walking frequency. Alternatively, it could be modified by introducing a constant offset to better represent real forces. Note that the speeds imposed during the tests ranged from slow to comfortable, but the performance of the models for fast speeds (above 1.4 m s^{-1}) was not tested. The data trends in Fig. 6 suggest that the errors could increase with speed, but this would require further tests for clarification.

3. Pedestrian force location tracking

Recommendations regarding the pedestrian force model based on a single point AHRS measurement were given in the previous section. However, in order to estimate correctly the influence of each pedestrian on bridge dynamics the location of the origin of the GRF vector (oGRF) needs to be established. Knowledge of pedestrians locations on a structure is also needed for analysing pedestrian–structure interaction, since the perceived vibration amplitudes depend on the local amplitude of the considered mode shape. The same information is required for analysing interactions between pedestrians, since the behaviour of each pedestrian might be affected by the behaviour of their neighbours. Therefore a detailed description of pedestrian force location tracking is given in this section. This work is timely as this issue has not been previously addressed in the context of research on human-induced vibration of structures. Furthermore, previous attempts at tracking pedestrian location from video footage [34–37] failed to accomplish this over long distances travelled by the pedestrians. Consequently assumptions of instantaneous pedestrian location are commonly made in response simulations, with the oGRF taken as equivalent to that position. The most common assumption is that of a linear relationship between mean values of walking velocity, v, step frequency, f_p, and step length, d:

$$v = f_p d \tag{4}$$

which neglects step-to-step variability. This can introduce inaccuracies in modal force estimation and cause discrepancies between the modelled and measured dynamic response. To alleviate this problem an algorithm for tracking the pedestrian's foot location based on data from AHRS and dead reckoning is presented in Sections 3.1 and 3.2. A novel algorithm is proposed in Section 3.3 which allows oGRF to be estimated from the same data, based on some simple assumptions.

3.1. Pedestrian tracking algorithm (dead reckoning)

Pedestrian dead reckoning (PDR) is a generic term describing relative (i.e. to a known reference) navigation techniques used to determine the position and orientation of a walker [38]. The input data for PDR usually comes from MEMS-based monitors attached to human body. Different methods of implementation of PDR are discussed elsewhere, e.g. [38]. The PDR algorithm used in this study was previously adopted in [39] and in principle relies on double integration of acceleration data from a monitor attached to a foot. The obtained translational motion is combined with orientation estimates from AHRS

gyroscopes and magnetometers that allow the direction of heading to be determined. The arrangement of the AHRS used for PDR is shown in Fig. 9 together with its LCS.

It is well known that numerical integration of noisy acceleration signals introduces drift. To reduce this effect the PDR algorithm exploits the bipedal nature of human gait. The gait cycle comprises two distinctive periods in which the leg is either in contact with the ground (i.e. stance phase) or swinging (i.e. swing phase). During stance phase the foot rolls from the heel to the toes, but there is a period during which it can be considered stationary. Identifying these periods allows zero-velocity updates (ZUPTs) to be applied which greatly improve the accuracy of estimates of translational foot motion [40].

The ZUPT starts with threshold detection in the acceleration magnitude:

$$|a| = \sqrt{a_{X,\mathrm{LCS}}^2 + a_{Y,\mathrm{LCS}}^2 + a_{Z,\mathrm{LCS}}^2} \tag{5}$$

below which the foot can be considered stationary, where the acceleration magnitude is previously relieved of the component due to gravitational acceleration. Although, in general, zero acceleration is not a sufficient condition for detecting zero velocity periods, it is reasonable to assume this relationship to hold for foot motion in walking. This can be understood from Fig. 10(a), containing raw acceleration output in LCS of a foot monitor (see Fig. 9) collected during a walking trial. The regions of constant (i.e. near zero) velocity are where the curves are flat and, after subtracting gravitational components, converge. This differs from a non-stationary period in foot motion, dominated by a leg swing, when the rate of change of acceleration is relatively high. Fig. 10(b) shows the corresponding acceleration magnitude data obtained with Eq. (5), treated with two-way second-order Butterworth low-pass filter with cut-off frequency 4.5 Hz. The beginnings and end of the identified non-stationary periods of foot motion, based on the threshold of 0.8 m s^{-2}, are denoted by circles and dots, respectively.

The raw monitor acceleration data in LCS are resolved to WCS with help of quaternions, then each acceleration signal is numerically integrated using the finite difference (mid-point) method and the values of velocity during the stationary period in foot motion are reset to zero. For each identified non-stationary period of foot motion a linear trend is next subtracted from the calculated velocity vector. This trend is constructed between a pair of data points in that vector corresponding to consecutive instances at which the foot motion is initiated and terminated, as can be seen in Fig. 10(b). Note these points are not equivalent to instances of stance phase and swing phase termination. Exemplar results of application of ZUPTs are presented in Fig. 11. The orientations of monitors in WCS are expressed relative to a North, West and vertical global reference frame and a velocity for each direction is calculated and presented in the plots from the top to the bottom, respectively. The drift in the velocity signals is visible in Fig. 11(a) containing data obtained by single integration of recorded

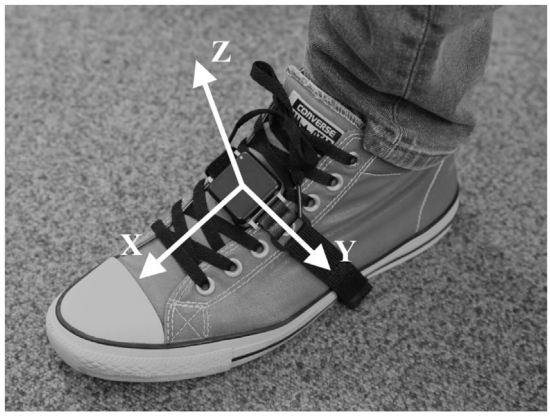

Fig. 9. AHRS attached to a foot, used for PDR. Three axes of LCS are denoted in white.

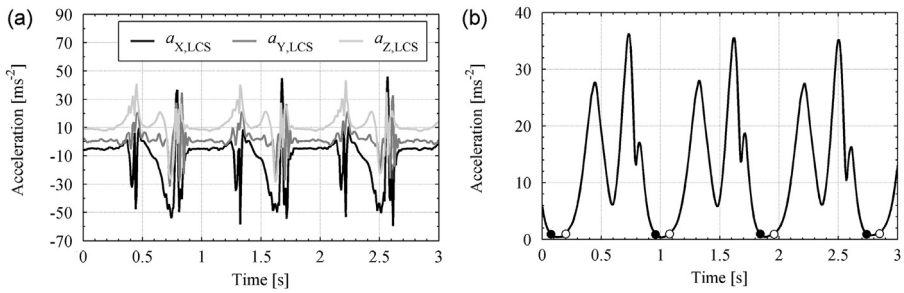

Fig. 10. (a) Raw acceleration signals in LCS measured during a walking trial. (b) Implementation of the threshold detection on acceleration magnitude data. Start and end of each non-stationary period in foot motion are marked by circle then dot.

acceleration signals. Fig. 11(b) shows the same data but obtained after applying ZUPTs. The difference between data in Fig. 11 (a) and (b) is caused by errors accumulated due to drift after approximately 30 s of walking.

Having performed ZUPTs, the velocity signals are integrated once more to obtain foot displacement in WCS. An exemplar outcome of this procedure is presented in Fig. 12. The data come from a test during which a subject was asked to walk between two lines drawn 30 m apart. The top plot shows the horizontal displacement of the instrumented foot relative to North and West. The subject was heading South-East in a fairly straight line. The middle plot shows vertical foot motion against the magnitude of horizontal displacement obtained by taking a square root of the sum of squares of data in the top plot, referred to as the distance travelled. The subject descended by approximately 0.35 m, corresponding to the average downward slope of the walking surface slope of 0.6 degrees. The bottom plot shows the magnitude of horizontal displacement against time. The distance of 30 m travelled by the walker is recovered with very good accuracy. The tangent to the average slope of the signal represents the walking velocity, which is approximately 1.5 m s^{-1}. The wavelike pattern of the signal composed of flat and inclined parts is a resultant of periods in which the foot is in contact with the ground and swinging, respectively.

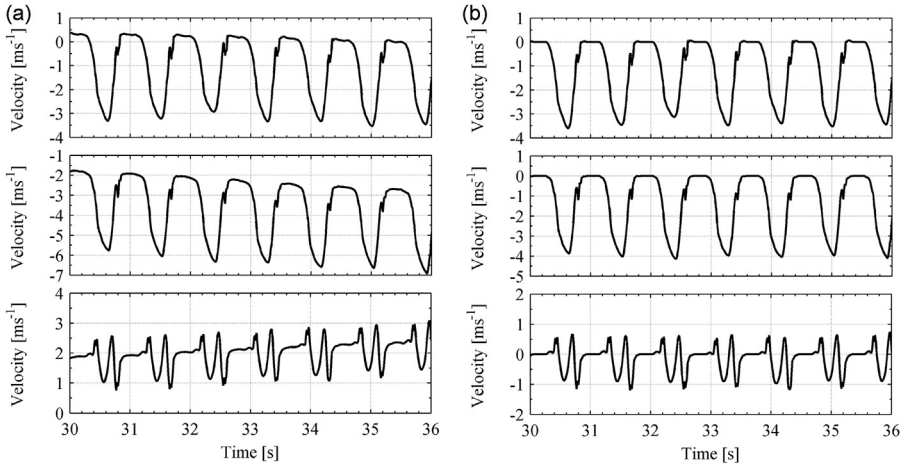

Fig. 11. Correction of drift in velocity signals using ZUPT. (a) Velocity signals obtained by integration of acceleration data. (b) Velocity signals corrected for drift. For (a) and (b) the two top plots correspond to North and West horizontal directions in WCS while the bottom plot corresponds to the vertical direction.

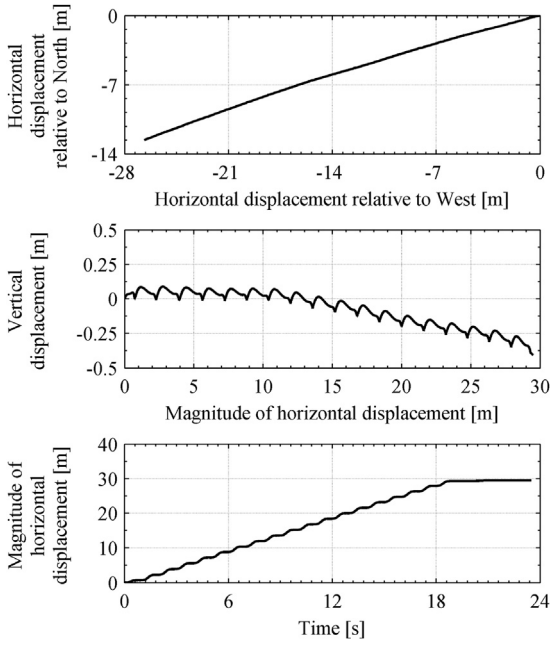

Fig. 12. Exemplar translational data of foot motion obtained with PDR.

3.2. PDR calibration and heuristic drift correction

Section 3.1 mentioned the importance to PDR of calibrating the acceleration magnitude threshold below which the foot can be considered stationary. The difficulty arises since the obtained acceleration amplitudes are affected by variations in monitor placement (in repeated deployment), the type of footwear worn, difference in foot motion patterns between individuals, etc. Therefore, rather than assigning one value and assuming its universal applicability, the threshold needs to be adjusted separately for each individual. In the case of a footbridge, having a clear direction of travel (including any gradient), walking a fixed distance provides a means to calibrate the threshold.

The algorithm only accounts for the lower harmonic components of motion because data from the monitored foot are low-pass filtered during PDR. Nevertheless, this feature does not compromise capability to capture real pedestrian behaviour since the spatio-temporal variability of motion patterns is preserved. Another important feature of the algorithm is that the direction of travel of the uninstrumented foot is implicitly assumed to be consistent with the longitudinal axis of the bridge. This is because it is the magnitude of horizontal foot displacement (e.g. shown at the bottom plot in Fig. 12) which is used for determining pedestrian location on the bridge. Any deviation of a pedestrian from a perfect straight, e.g. due to veering (see [9] for discussion of this), could reasonably be taken as random so as to increase actual distance travelled approximately evenly along the path. In this case a simple correction can be applied using the known straight line distance.

3.3. Determination of the origin of ground reaction force vector (oGRF)

Determining the precise location of oGRF typically requires either a force plate, appropriately arranged instrumented treadmill, instrumented insoles, pressure mats or shoes instrumented with force cells. Only the latter two methods offer capabilities of identifying oGRF in normal overground walking over long distances. However, even data collected using the latter two methods, if used alone, are not fit for purpose since the obtained oGRF is expressed relative to the position of the foot, whose coordinates relative to the structure are unknown. Therefore in this study, to keep the instrumentation simple, a novel algorithm for the determination of approximate (i.e. pseudo) location of oGRF was developed in which output of PDR is used as an input.

As with PDR, the main idea behind the oGRF identification algorithm derives from the bipedal nature of human gait. During a single support phase, oGRF is located within the boundaries of the foot in contact with the ground. During a double support, when body weight shifts to the contralateral (i.e. stepping) leg, oGRF travels to the location of the foot of that stepping leg.

Algorithm implementation requires information on the motion of both feet. Putting one monitor on each foot would satisfy this requirement, however, this would require three monitors per pedestrian, i.e. one to estimate the force and one monitor on each foot (the tasks described in Sections 3.3.1 and 3.3.2 can then be skipped). In the situation where the number of monitors is limited, one-third reduction in instrumentation can be achieved by instrumenting one foot only, thus allowing larger pedestrian groups to be studied. To that end, a three-stage method allowing the motion of the uninstrumented foot to be synthesised is presented and its performance is analysed. The first stage (Section 3.3.1) determines positions and locations where the uninstrumented foot can be considered stationary (i.e. flat on the ground) and the second stage (Section 3.3.2) determines trajectories of the uninstrumented foot during non-stationary periods. To ensure smooth transition between stationary and nonstationary periods, Section 3.3.3 stitches the patterns together to produce a smooth continuous motion pattern (trajectory). The reconstruction process was checked using data obtained with both feet instrumented with AHRS, by reconstructing the motion of one foot based on data from the other foot and yielded satisfactory results. Once the information on the motion of both feet is available, double support phases of gait can be identified, allowing oGRF tracking in time and space (Section 3.3.4).

3.3.1. Stationary periods in uninstrumented foot motion

Positions where the uninstrumented foot is stationary are effectively estimated by assuming they are equidistant between successive stationary locations of the instrumented foot obtained by PDR, as indicated in Fig. 13(a). The black curve in Fig. 13(a) shows the distance travelled by the instrumented foot, taken as the magnitude of horizontal foot displacement obtained with PDR (see Section 3.2), plotted with respect to time.

The plateaus evident in the plot, denoted by segments AB, CD and EF with circles and dots marking their beginnings and ends, respectively, are when the instrumented foot is stationary. The midpoints between the plateaus are then identified, which split the distance travelled during a step into two equal lengths. For example, the midpoint in distance travelled during a step in which the foot moved from AB to CD is denoted by ab. The modulus of the difference between the ordinates (distance) of two consecutive midpoints (e.g. ab to cd) is assumed to be the distance travelled by the uninstrumented foot during a step.

Durations of plateaus for uninstrumented foot are taken as the average of the durations of the two plateaus immediately surrounding the associated midpoints for the instrumented foot. The plateaus corresponding to the uninstrumented foot are assumed to occur at times such that abscissas (timing) of their midpoints fall at the corresponding abscissas of midpoints of the non-stationary periods of instrumented foot data. The equations describing the location of midpoints (S) and their durations (T) are given in Fig. 13.

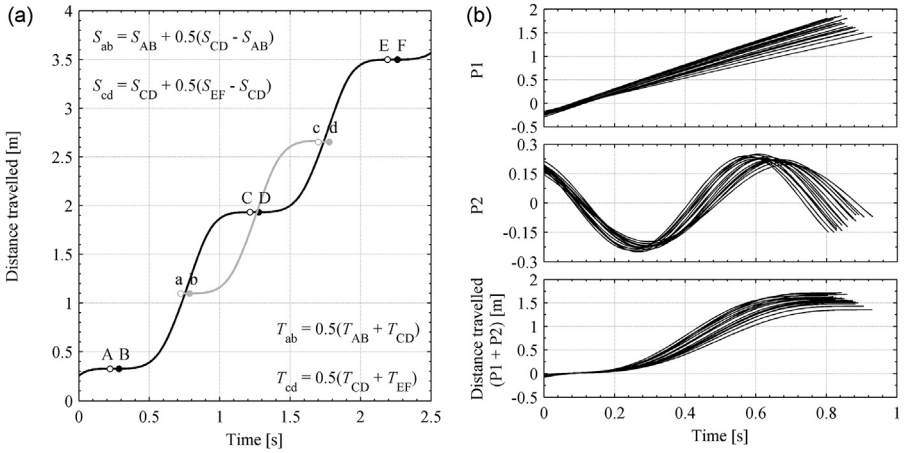

Fig. 13. (a) Reconstruction of stationary periods in the uninstrumented foot motion. The measured position of the instrumented foot is denoted by a black curve. The segments AB, CD and EF are the identified plateaus in instrumented foot data. The segments ab and cd denoted in grey are the reconstructed plateaus for the uninstrumented foot. Formulae for spatial location (S) and duration (T) of those segments are given on the plot. For all data, circles and dots mark the beginnings and ends of plateaus, respectively. The grey curve describes the motion of the uninstrumented foot during non-stationary period. (b) Exemplar performance of fitting Eq. (6) for non-stationary periods of the instrumented foot motion.

3.3.2. *Non-stationary periods in uninstrumented foot motion*

Reconstruction of the non-stationary period of the uninstrumented foot motion (e.g. segment bc in Fig. 13(a)) is based on finding a suitable fit $k(t)$ to the trajectory of the non-stationary period of the instrumented foot motion (e.g. segments BC and DE in Fig. 13(a)). A suitable form for $k(t)$ is the sum of two sinusoidal components:

$$k(t) = \underbrace{\alpha_1 \sin(\alpha_2 t + \alpha_3)}_{\text{P1}} + \underbrace{\beta_1 \sin(\beta_2 t + \beta_3)}_{\text{P2}} \tag{6}$$

where $\alpha_1, \alpha_2, \alpha_3, \beta_1, \beta_2$ and β_3 are coefficients to be determined. The parts of the function characterised by slow and fast oscillation, referred to as P1 and P2 respectively, reflect the horizontal progression of the foot and its swinging motion. This can be seen in Fig. 13(b) presenting fitted data for non-stationary periods of the instrumented foot for a subject with $m_p = 81$ kg and $h = 1.83$ m walking the distance of 30 m at variable speed, i.e. purposely increasing and decreasing their velocity to provide a test of the algorithm. For the record of which a truncated time history is shown in Fig. 13(a), the goodness of fit statistics expressed in terms of the average adjusted R-square and standard error, based on fitting to 72 steps collected during a single trial, are 0.999 and 0.005 m, respectively. Similar goodness of fit statistics were obtained for all other analysed data regardless of the speed of travel of the walker and their pacing frequency.

Having shown that the function in Eq. (6) provides a good estimation of the motion of the instrumented foot, the next step is to apply this to reconstruct corresponding non-stationary period of uninstrumented foot motion. To this end the coefficients of P1 and P2 (i.e. $\alpha_1, \alpha_2, \alpha_3, \beta_1, \beta_2$ and β_3) need to be known a priori. Therefore tests were conducted in which seven people walked a known distance at different speeds with AHRS monitors attached to their feet. The dependence of the coefficients of Eq. (6) on the duration of and distance travelled during non-stationary periods in foot motion was investigated. An example is presented in Fig. 14, showing data from a single test during which a subject was asked to walk with a variable speed over the distance of 150 m. The best second-order polynomial surface fits to the data are denoted in grey. The amplitude β_1 and angular frequencies α_2 & β_2 show a strong dependence on duration and distance with adjusted R-square values typically above 0.92 and standard errors for these coefficients below 0.06, 0.005 rad/s and 0.15 rad/s, respectively. Fig. 14 shows lower accuracy for fitting amplitude α_1 and invariance of phase angle α_3 & β_3. The low variability of these coefficients relative to the range of phase angle indicates that their mean values can be taken as applicable generally for the tested subject. This observation is substantiated by data in Fig. 13(b) showing that the patterns of evolution of two sinusoidal components of Eq. (6) (P1 and P2) are similar for all fits, although the duration and distance travelled might vary.

Analyses of data collected during a series of tests have shown that the coefficients of Eq. (6) should be calibrated for each subject separately because of inter-subject variability of foot motion pattern and monitor placement (see Section 3.2). However, reconstruction of a foot motion pattern based on coefficients drawn from polynomial fits, even if derived separately for each subject, is prone to inaccuracies as the mutual dependence of these coefficients is unlikely to be captured perfectly. Therefore, two additional steps implemented in the algorithm to correct for this effect are described in the next section.

3.3.3. *Stitching together time histories for stationary and non-stationary trajectory components for uninstrumented foot*

Now having identified constructed time history components corresponding to moving and stationary uninstrumented foot, two minor additional steps (which a busy reader could skip) are needed to arrive at a kinematically correct complete time history of uninstrumented foot motion. The first step adjusts the shape at the ends of a trajectory component for the

foot moving, so as to ensure smooth landing at zero velocity. The second step uniformly scales (in distance axis) the trajectory to correct for small discontinuities in position resulting from the first step.

The nature of the fitted function for the moving foot trajectory does not guarantee monotonic increase where it meets the (level) plateau representing the stationary foot. Points of inflection in the reconstructed (moving) foot trajectory are identified via local minima in the first derivative (velocity, which should be zero). Fig. 15 is an example where the points of inflection of the reconstructed (grey) curve in Fig. 15(a) are identified by black dots at 0.37 s and 1.24 s via the first derivative (velocity) shown in Fig. 15(b). Zooming on Fig. 15(a) shows the fitted trajectory to have a turning point just before the point of inflection at 1.24 s. After this point (marked as a black dot) the fit suggests that the foot moves backward. To correct for this, the reconstructed foot motion pattern is simply linearised at the ends. This is performed for the range of data from the most inward points defined either by points of inflection or, if they exist (such as on the plot in Fig. 15(a)), local minimum or maximum outwards such that the ends are flat (black lines in the insets of Fig. 15(a)).

The inserts in Fig. 15(a) show that the ends of the corrected patterns (black lines) are displaced with respect to the (stationary) plateaus (grey lines). Therefore in the second step the distance travelled during the reconstructed motion pattern is scaled up or down, stretching or compressing motion pattern in space (rather than time), after which the pattern is realigned between the corresponding plateaus.

The accuracy of the described procedures can be inspected in Fig. 15(c). To create this figure an experiment was conducted where monitors were placed on both feet of the pedestrian. The solid black curve shows the measured foot motion (in this case the right foot) and the dashed black curve shows the measured contralateral (left) foot motion. The solid grey curve shows the reconstructed motion of the right foot based on the observed motion of the contralateral (left) foot and the approach presented in Sections 3.3.1–3.3.3. Fig. 15(c) shows that, broadly speaking, there is a good match between the measured foot motion and the reconstructed foot motion. The Pearson's linear correlation coefficient, calculated after detrending each signal with its linear fit, is 0.97. The lowest values of this coefficient (but still above 0.95) were obtained for tests in which the subjects were asked to walk with variable speed, i.e. deliberately increasing and decreasing their velocity.

3.3.4. *Determination of the double support phase of gait and oGRF*

The next step in the proposed algorithm determines double support phases of gait within the analysed data. Since this information cannot be obtained directly using AHRS, a suitable method was developed using the data from the treadmill experiments to establish a relationship between the walking frequency and duration of double support phase of gait. Stride durations, taken between two consecutive TOs of the same leg, were quantified after discarding the range of data associated with gait inception and termination stages. The durations of two double-support phases of gait occurring within each of those strides were then calculated. The relationship between the percentage duration of double support phase, expressed in relation to stride duration, and pacing frequency is presented in Fig. 16. The data are based on averages from strides marked by TOs of right and left legs.

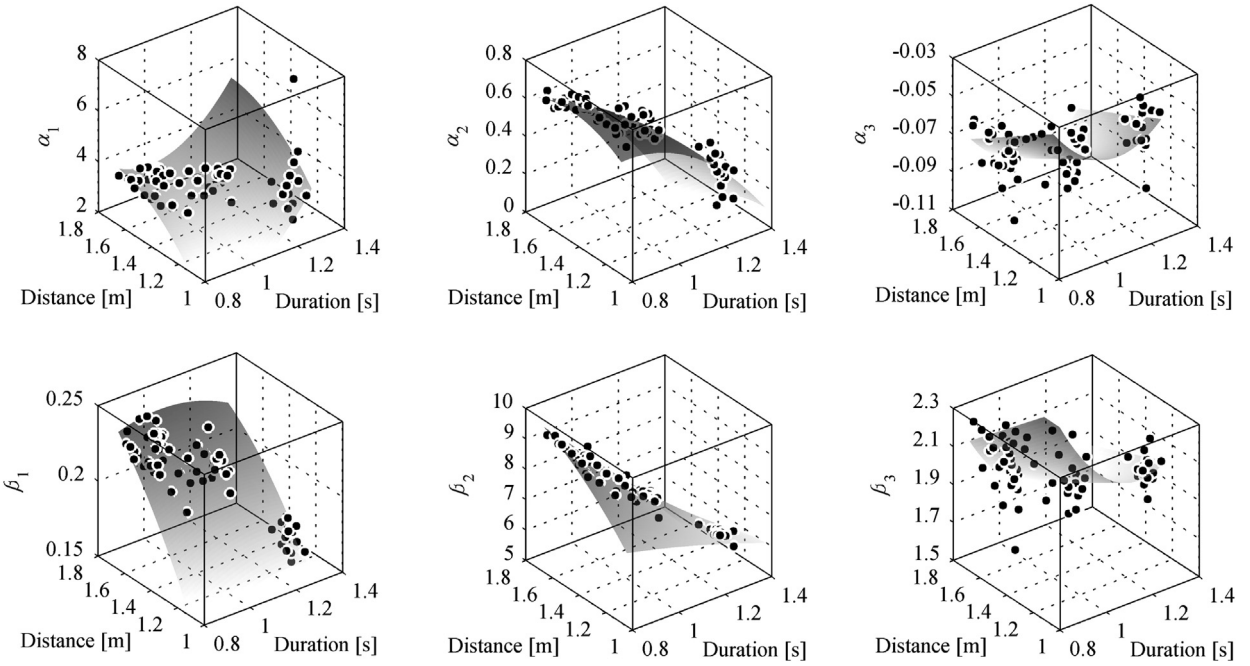

Fig. 14. Exemplar coefficients of the fit described by Eq. (6) based on data from one foot derived for a subject with $m_p = 81$ kg and $h = 1.83$ m walking the distance of 150 m at variable speed. The best polynomial surface fit is shown for each coefficient.

As in the case of the percentage error in Fourier force amplitude corresponding to the pacing frequency presented in Figs. 6 and 7, subject specific trends can be seen in data in Fig. 16. In order to show the average trend in all data for all subjects, a fit based on power law relationship was calculated:

$$T_{DS} = -0.015 f_p^{2.571} + 0.366 \tag{7}$$

where T_{DS} is expressed as a percentage of stride duration.

It is reasonable to assume that the double support phase of gait occurs periodically when the two feet are the furthest apart. After identifying these points in foot motion data, stride durations corresponding to these points are established by taking the period between the ends of two plateaus in instrumented foot motion containing considered double-supports. A reciprocal of stride duration is assumed to be equal to the instantaneous stride frequency, which is half the pacing rate. Having established the instantaneous pacing rate, the duration of the double support phase of gait is calculated from Eq. (7). Double supports are assumed to occur symmetrically around the identified points where the feet are the furthest distance apart. Exemplar performance of the proposed algorithm for determining oGRF is presented in Fig. 17. The regions corresponding to double support phase of gait are shaded in grey and the evolution of the location of oGRF is shown as a thick black curve. The curvature of foot motion patterns during double support periods is associated with progression of a foot during roll-over.

The performance of the proposed pedestrian force location tracking method will be further discussed in Section 5, reporting results of a study performed to show the applicability of the proposed framework. The experimental campaign used to gather data on pedestrian and bridge behaviour is described next.

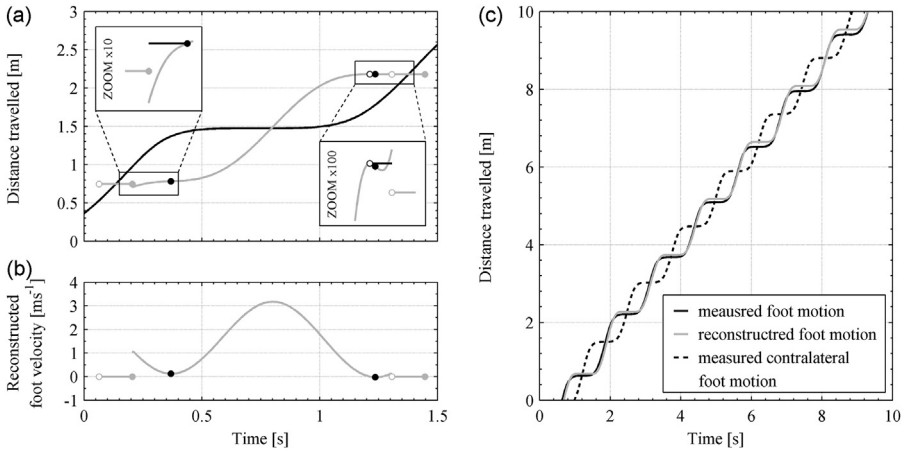

Fig. 15. (a) Motion patterns measured on instrumented foot (black curves) and reconstructed for uninstrumented foot (grey curves). (b) The first derivative of the reconstructed pattern of uninstrumented foot motion in (a). Black dots marking local minima in (b) correspond to points of inflection in uninstrumented foot data in (a). Grey circles and dots in (a) and (b) mark the beginnings and ends of the plateaus representing stationary periods in foot motion. Black circles in (a) correspond to the local maximum in reconstructed foot motion. Black lines on zoomed-in subplots in (a) represent linearised ends in the reconstructed motion pattern. (c) Comparison of measured and reconstructed of foot motion.

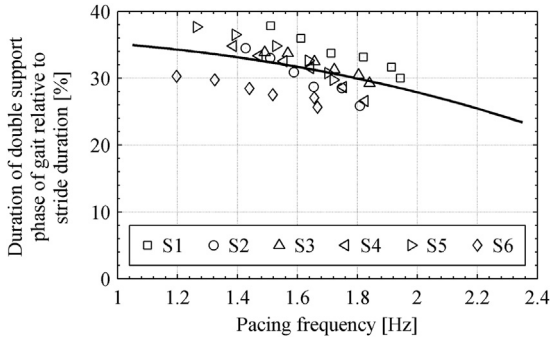

Fig. 16. Percentage duration of double support phase of gait, expressed in relation to stride duration, against pacing frequency. The trend in data described by Eq. (7) is shown as a black curve.

4. In-situ testing on a full-scale structure

Controlled pedestrian loading tests were performed on Baker Bridge (BB) in Exeter, UK. BB was constructed in 2008 and is located close to the Sandy Park Stadium (50°42′38.6″N 3°28′13.3″W) which is the home ground of the Exeter Chiefs rugby team. The bridge (see Fig. 18) crosses a dual carriageway and has total length approximately 108.6 m with main span (South end) and back span (North end) having approximate lengths of 71.285 m and 37.36 m, respectively. The 42 m high steel A-frame tower supports the ladder deck via six pairs of cable stays with another pair of cable stays anchored at the North abutment. The deck has two continuous longitudinal steel main beams pinned at the North abutment, resting on a tower crossbeam via pad bearings and having a sliding expansion joint at the South abutment.

BB deck is at least 10 m above the ground throughout most of its span and has a downward North-to-South slope of approximately 2.79°, causing 5.3 m difference in the footway levels at the ends of the bridge. The footway is a 3 m wide concrete slab enclosed by 1.4 m high steel parapets. An estimated total 49 t of steel and 98 t of concrete were used in the deck construction.

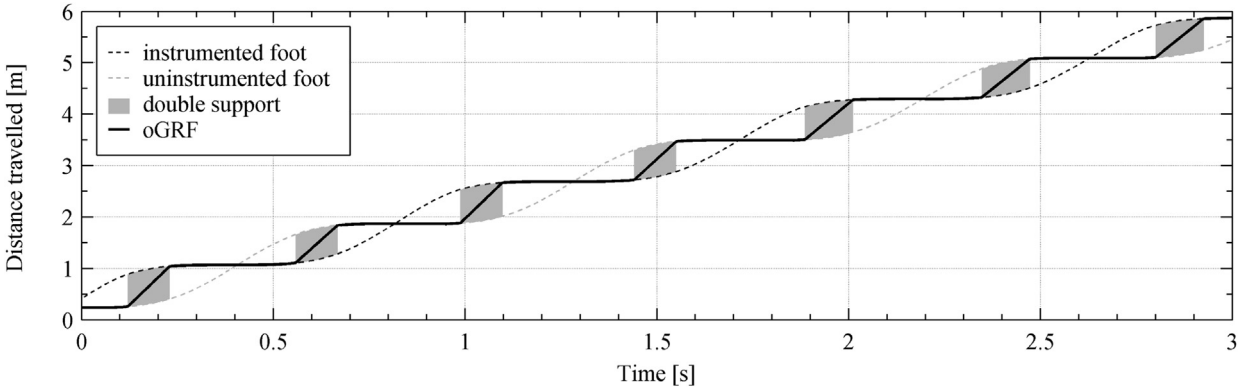

Fig. 17. Exemplar performance of the proposed algorithm for the determination of the origin of ground reaction force vector.

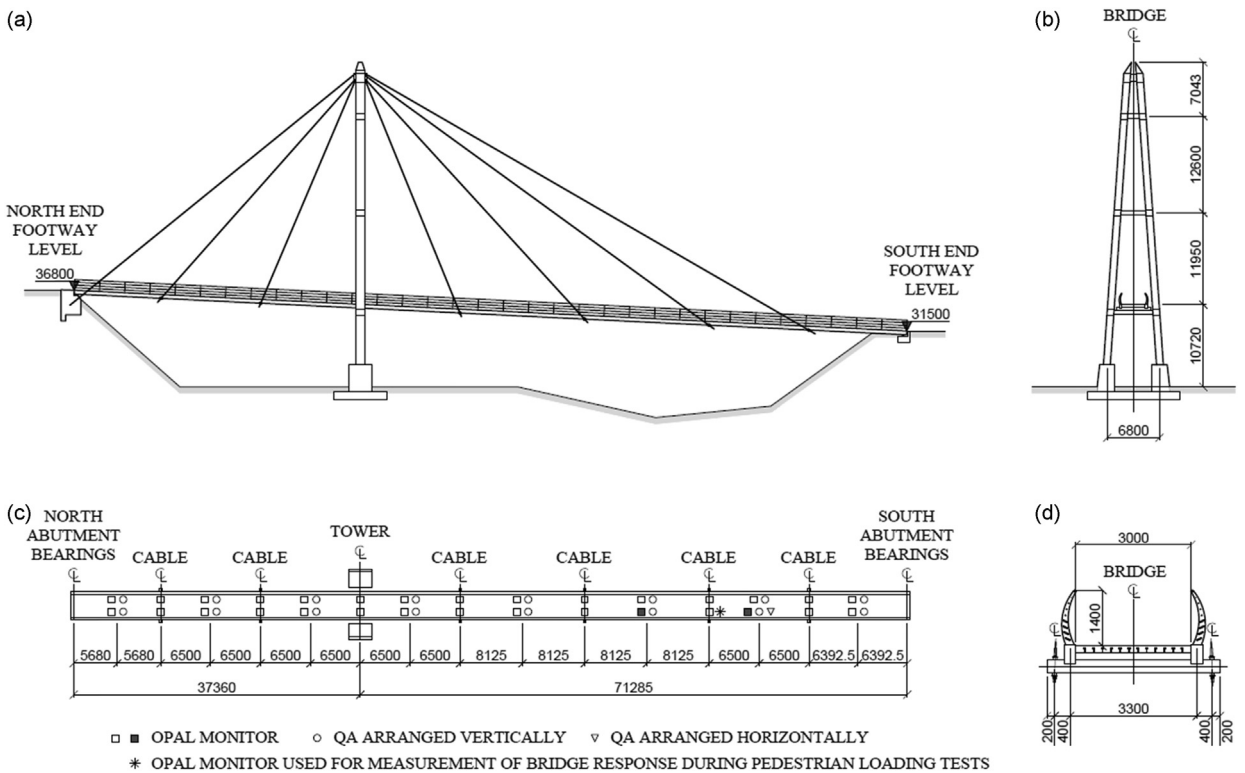

Fig. 18. (a) Elevation and (b) cross-section through the tower of Baker Bridge. (c) The true plan on deck together with instrumentation layout. The roving and reference Opal™ monitors are denoted by empty and filled squares, respectively. (d) A cross-section through the deck.

A dedicated modal testing campaign conducted to obtain modal properties of the empty bridge is described in the next section.

4.1. Modal testing

Two instrumentation systems were deployed in order to determine BB modal parameters i.e. natural frequencies, damping ratios and mode shapes. These were a set of six Opal™ monitors and an array of conventional wired Honeywell QA quartz-flex low noise servo-accelerometers used to cross-check the more noisy data from the Opal™ AHRS monitors. One QA (see Fig. 18(c)) was set horizontally to check for coupled cross-axes modes. The ambient vibration testing performed with AHRS used a standard method of allocating reference and roving accelerometers. The method is the same as used on Humber Bridge [41], and provided the definitive set of BB mode shapes, shown in Fig. 19.

Parameter estimates obtained from ambient testing are known to exhibit significant variance [42], so specific and more reliable parameter values appropriate to the level of response due to a pedestrian were obtained by further measurements using a force plate and an instrumented hammer. The force plate was used to record vertical forces during short sequences of up to eight jumps prompted by a metronome set to a bridge natural frequency estimated in the ambient tests. The free decay of response to jumping was used to extract accurate damping and frequency values via curve fitting to exponentially decaying sinusoids [43].

Additionally, single degree of freedom circle fitting to the frequency response function of acceleration to force derived from jumping tests was used to estimate modal masses, using hammer testing to cross-check values. Modal mass values are based on mode shapes having maximum vertical mode shape ordinate set to unity, and are applicable for loads applied at any point of the deck for modes 1–4 and along the walkway edge for mode 5.

The modal parameter values appropriate for response calculations are given in Table 3. The inherent damping ratios for all the presented modes are relatively low [44].

Mode 2 and 3 frequencies correspond to pacing rates which can be expected in the case of relaxed walking e.g. for a crowd on a match day, and the case of normal walking, respectively. Therefore, the controlled pedestrian loading tests focused on the behaviour of BB at frequencies of these two modes.

4.2. Controlled pedestrian loading tests

To assess the loading model introduced in Section 2 and the algorithm for the pedestrian force location tracking introduced in Section 3, a series of tests with a single walker was performed on BB. Monitors were attached at the sternum, navel, lower back, C7 and one foot. The test subject (a 34 years old male, $m_p = 81$ kg and $h = 1.83$ m) was asked to walk to the rhythm of a metronome set to 1.6 or 2 beats per second, corresponding to the frequencies of modes 2 and 3, respectively (see Table 3). Each test started from the subject standing still at a line marked 1 m behind the bridge end (i.e. outside of the boundary of the deck). The subject was asked to terminate gait 1 m behind the other end of the bridge, at a marked line. This allowed the duration of and the distance travelled (110.6 m) during a test to be easily identified in the AHRS data. Two tests were performed at each metronome rate in which the pedestrian walked either from North to South or from South to North across the bridge. This was to investigate if the slope of the bridge has any effect on the results. The response of the bridge to the walker was measured by the monitor placed at the location denoted in Fig. 19(c) by a star. The results of the controlled

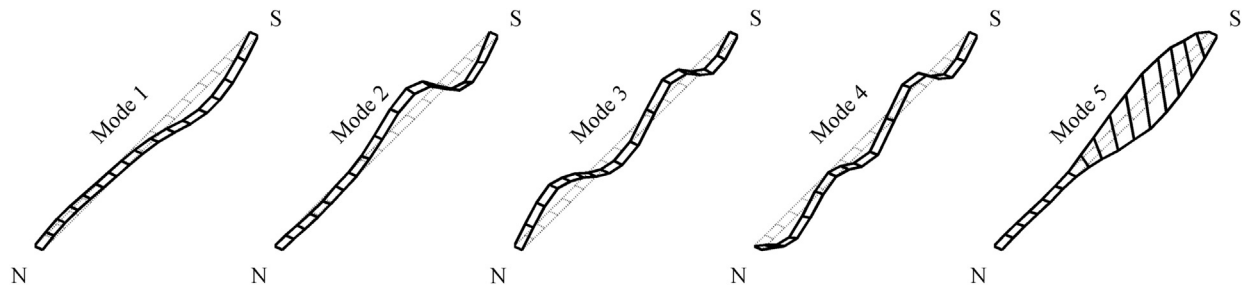

Fig. 19. The first five lowest identified mode shapes of Baker Bridge. North and South ends of the bridge are denoted by N and S, respectively.

Table 3
Modal properties of Baker Bridge for the first four lowest vertical modes and the first torsional mode.

	Mode 1	Mode 2	Mode 3	Mode 4	Mode 5
Frequency, f_n [Hz]	0.94	1.61	2.00	2.24	2.84
Modal mass, M_n [tonne]	55	68.4	57.2	57.3	40
Damping ratio, ζ_n [%]	0.16	0.19	0.32	0.37	0.22

pedestrian loading tests are reported in the next section, comparing the measured bridge response and the response simulated using the proposed framework.

5. A study comparing measured and simulated bridge response

Having introduced the procedures leading to reconstruction of pedestrian force (Section 2) and its instantaneous location (Section 3), this section examines how successful these procedures are at simulating footbridge response. A modal model of BB is built using information from Section 4.1, to which pedestrian force is applied. The location of this force is taken either as moving at a constant speed along the bridge or equal to oGRF (see Section 3.3).

The flowchart in Fig. 20 presents a graphical summary of the proposed framework. The last and standard step, represented in the lower right of the figure, is calculating bridge response to moving and mode-shape modulated pedestrian force. The following equation of motion can be written for each mode:

$$\ddot{X}(t)+2\zeta_n\omega_n\dot{X}(t)+\omega_n^2X(t)=\frac{1}{M_n}\sum_{i=1}^{N}F_i(t,x_i)\phi_{i,n}(x_i) \tag{8}$$

where X is the modal displacement, ζ_n is the damping ratio, ω_n is the natural frequency, M_n is the modal mass, F_i is the force amplitude of the $i-$th pedestrian, N is the total number of pedestrians on the bridge, $\phi_{i,n}$ is the amplitude of the $n-th$ mode shape at $i-$th pedestrian location, x_i is the ith pedestrian location, and dots over symbols represent relative differentiation with respect to time t.

5.1. Response of the bridge to a single pedestrian

In this section the measured response of the bridge subjected to loading from a single walking pedestrian is compared to the response predicted by the proposed framework. The simulated and measured vertical responses in mode 2 and mode 3 for the pedestrian walking at 1.6 Hz (chosen to directly excite mode 2) and at 2 Hz (chosen to directly excite mode 3), respectively, are shown in Figs. 21 and 22. For each mode, the measured response was band pass filtered with two-way fourth-order Butterworth low-pass filter with cut-off frequencies $f_n \pm 0.1$Hz. The data in Figs. 21 and 22(a) are from tests in which the pedestrian was walking from the North to the South end of the bridge, and in Figs. 21 and 22(b) from tests in

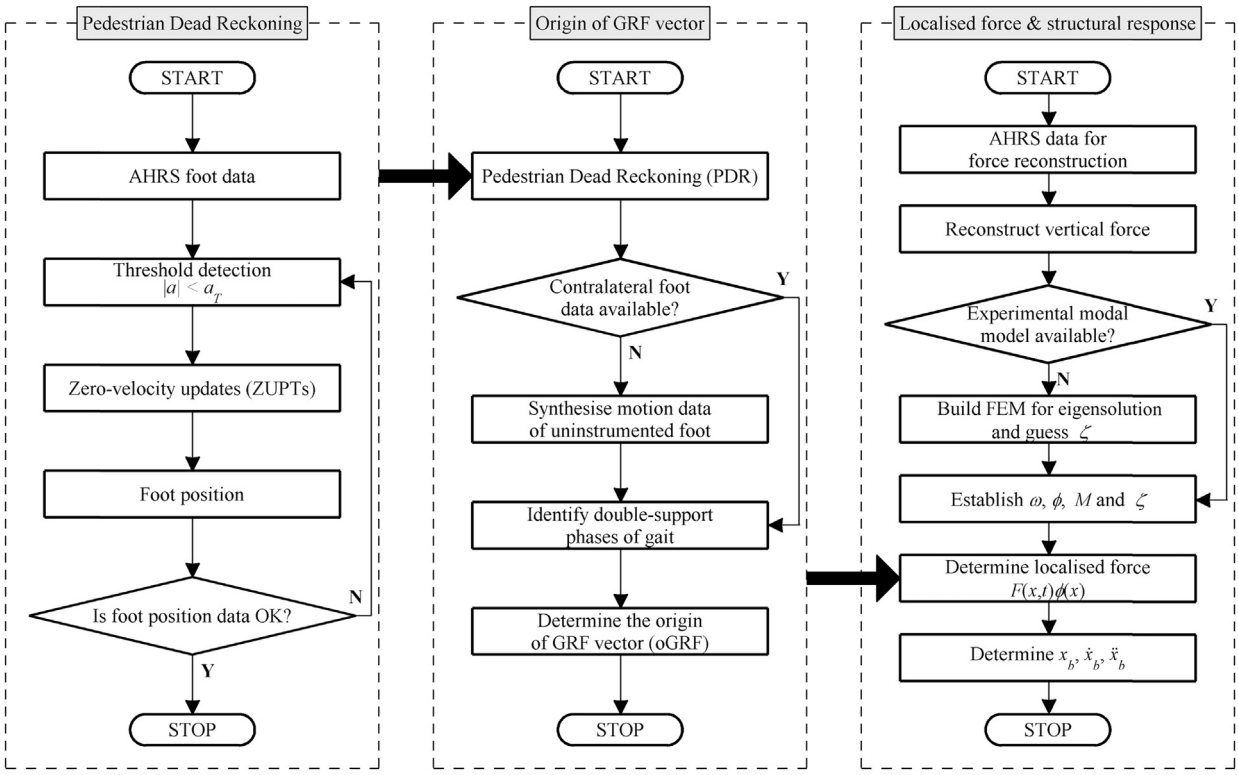

Fig. 20. A flowchart showing the proposed framework for the determination of localised pedestrian forces on full-scale structures using attitude and heading reference systems.

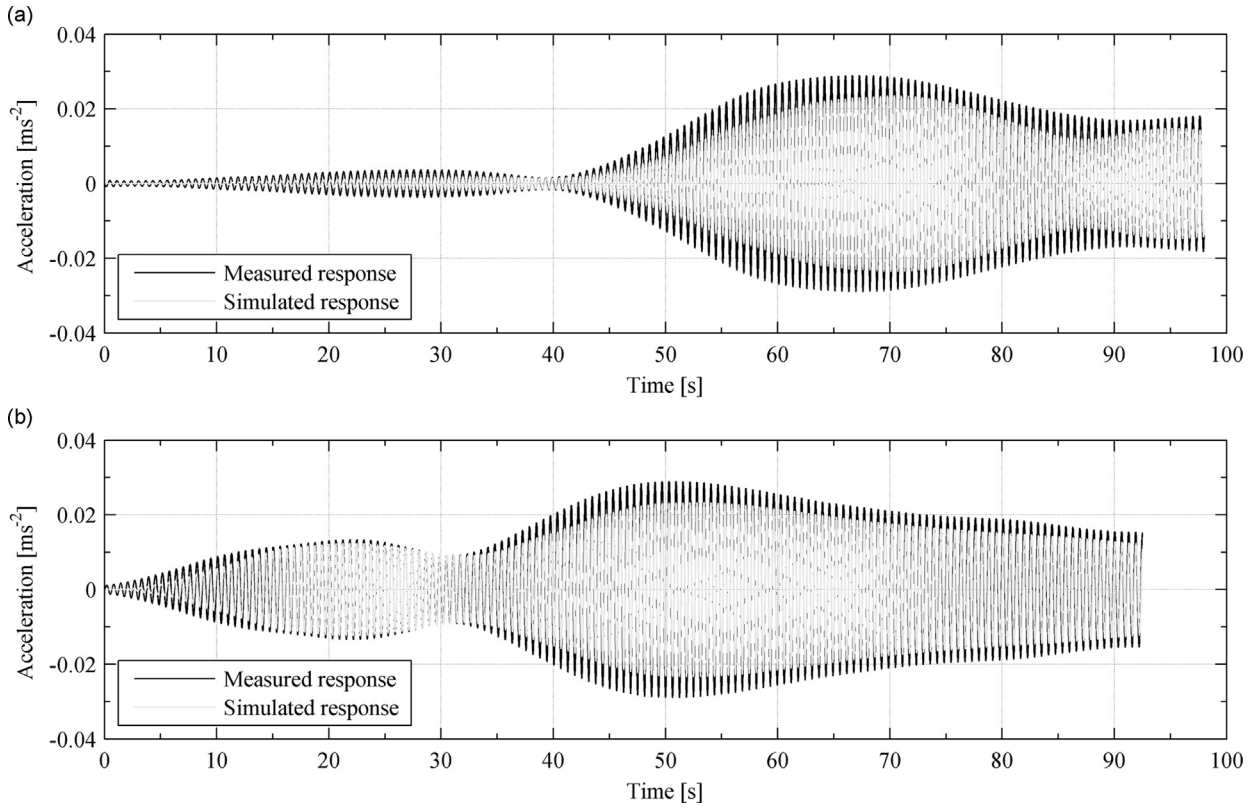

Fig. 21. Simulated and measured response of Baker Bridge in mode 2 ($f_n = 1.61$Hz, $\zeta_n = 0.19\%$, $M_n = 68.4 \times 10^3$kg), for a pedestrian walking at 1.6 Hz (a) from the North to the South end of the bridge, and (b) from the South to the North end of the bridge.

which the pedestrian was walking from the South to the North end of the bridge. The lengths of signals presented in Figs. 21 and 22 correspond to the duration of the respective tests. All simulated data presented in Figs. 21 and 22 are based on force reconstructed from monitors attached at C7.

The maximum measured acceleration amplitudes in Figs. 21 and 22 are just below 0.03 m s^{-2} and 0.2 m s^{-2}, respectively. The maximum acceleration amplitudes at the antinodes of mode 2 and mode 3 are 0.05 m s^{-2} and 0.37 m s^{-2}, respectively. This shows that the bridge can exhibit lively behaviour (i.e. large amplitude response) under the action of walking pedestrians but its response is acceptable according to the guidance at the time of construction [45].

Fig. 21 shows that the simulated response amplitudes for mode 2 generally underestimate the measured response. A converse relationship can be seen for mode 3 in Fig. 22. However, the patterns of evolution of the amplitude of simulated response generally follow the measured data well. The maximum response amplitudes in mode 2 are approximately an order of magnitude lower than in mode 3.

A detailed comparison between the measured and simulated results based on force reconstructed using AHRS data from different body landmarks is presented in Table 4. Three performance indices are given: percentage difference in maximum acceleration amplitude relative to the measured data, average RMS error in the envelope of acceleration amplitude and Pearson's linear correlation coefficient. The last two indices were calculated after discarding the first 10 s of the signal due to the effect of initial conditions. Normal and italic font styles denote the results obtained by assuming a constant walking speed and using the algorithm for tracking oGRF, respectively. For brevity, the tests with the subject's pacing rate corresponding closely to modes 2 & 3 frequencies are referred to as T1, T2 & T3 and T4, respectively. The direction of travel was from the North to the South end of the bridge for T1 and T3 (i.e. downhill walking) and from the South to the North end of the bridge for T2 and T4 (i.e. uphill walking). The average walking speeds during T1, T2, T3 and T4 were, respectively, 1.13 m s^{-1}, 1.2 m s^{-1}, 1.64 m s^{-1} and 1.61 m s^{-1}.

A strong linear correlation between the measured and simulated response of the bridge has been found for all cases, with positive values of Pearson's linear correlation coefficients in Table 4 indicating in-phase relationships. Figs. 21 and 22 indeed show that the peaks in the measured response and the response simulated based on data from C7, occurring at the intervals equal to reciprocal of the modal frequencies, are aligned in time reasonably well.

5.1.1. Results for T1 and T2 (mode 2)

Examination of differences in maximum acceleration amplitude in Table 4 shows that the simulated data generally underestimate the maximum acceleration amplitudes for T1 and T2. This is the most pronounced for LB, which agrees with

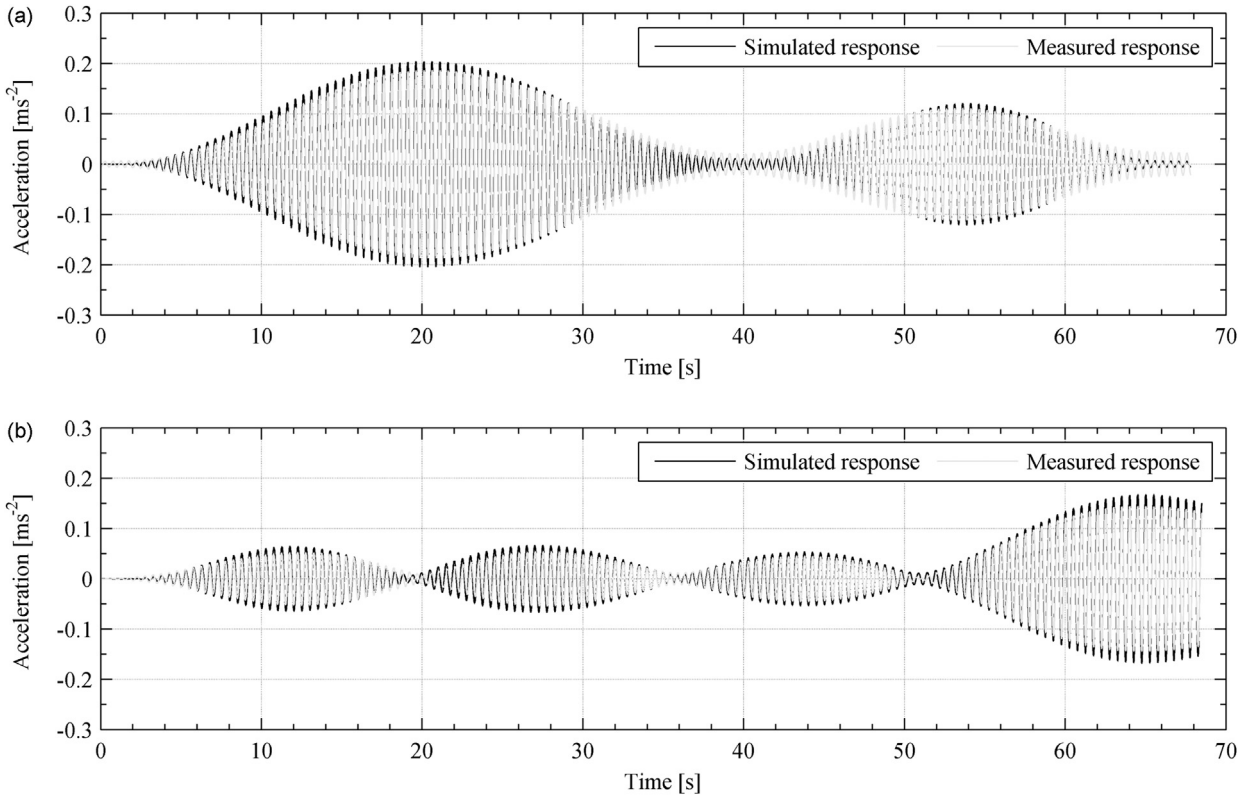

Fig. 22. Simulated and measured response of Baker Bridge in mode 3 ($f_n = 2$Hz, $\zeta_n = 0.32\%$, $M_n = 57.2 \times 10^3$kg), for a pedestrian walking at 2 Hz (a) from the North to the South end of the bridge, and (b) from the South to the North end of the bridge.

the results in Figs. 6 and 7(a) showing that the largest error in the amplitude of the Fourier component of force for $f_p = 1.6$Hz and $v \in \langle 1.13;1.2 \rangle$ m s^{-1} can be expected from a model based on data collected from this body landmark. However, while the negative difference in maximum acceleration amplitude is consistent with data presented in Section 2 for LB, a positive difference would be more likely for N and S. Interestingly, the simulation results obtained using oGRF are less accurate than those obtained assuming a constant walker speed. The average absolute difference in maximum acceleration amplitude relative to the measured data for all models using oGRF is approximately 43 percent, compared with 30 percent obtained from models assuming a constant walker speed. The best accuracy in terms of the maximum response amplitude for T1 and T2 is found for N and S, respectively, which underestimate the measured response by 22.8 percent and 13.7 percent. The maximum average RMS envelope error for T1 and T2 is 0.008 m s^{-2} for LB. This value stands at 26 percent relative to the maximum acceleration amplitudes for T1 and T2, respectively, measured at 0.029 m s^{-2} in both tests.

5.1.2. Results for T3 and T4 (mode 3)

Better performance of the framework is evidenced for T3 and T4. All models assuming a constant walker speed tend to overestimate maximum acceleration amplitudes, which seems to be consistent with data in Figs. 6 and 7. The least and greatest differences for both T3 and T4 are found for LB and S, respectively. The simulation results obtained using oGRF improve the match with the maximum measured response, except for LB in case of T3, most often changing sign of the difference, i.e. resulting in underestimated vibration amplitudes. The average absolute difference relative to the measured data for all models using oGRF is approximately 7 percent, compared with 12 percent obtained for models assuming a constant walker speed. Best accuracy in terms of the maximum response amplitude for T3 and T4 based on results obtained using oGRF is found for S and C7, respectively, which underestimate the measured response by 2.9 percent and 3.4 percent. The maximum average RMS envelope error for T3 and T4 is, respectively, 0.021 m s^{-2} for LB and 0.006 m s^{-2} for S. These values stand at 11.34 percent and 4.21 percent relative to the maximum acceleration amplitudes for T1 and T2, respectively, measured at 0.187 m s^{-2} and 0.145 m s^{-2}.

5.2. Discussion

Test results demonstrate the feasibility of the proposed methodology. A satisfactory agreement between simulated and measured responses has been found for all the force models (LB, N, S, C7) and both the force localisation procedures (constant velocity & oGRF). A Pearson's linear correlation coefficient higher than 0.94 was found in all cases, corresponding

Table 4
Performance indices for simulated response of BB for walking tests with a single pedestrian. The results are representative of the pedestrian loading reconstruction procedure based on data from AHRS attached at LB, N, S and C7. Normal and italic font styles denote the results obtained by assuming a constant speed of the walker and using the algorithm for tracking oGRF, respectively.

Performance indices	**T1** mode 2 North→South				**T2** mode 2 South→North				**T3** mode 3 North→South				**T4** mode 3 South→North			
	LB	**N**	**S**	**C7**	**LB**	**N**	**S**	**C7**	**LB**	**N**	**S**	**C7**	**LB**	**N**	**S**	**C7**
Difference in maximum acceleration amplitude [%]	−46.2 *−59.5*	−22.8 *−32.8*	−36.1 *−47.7*	−29.9 *−41.6*	−40.4 *−58.1*	−24.0 *−39.3*	−13.7 *−27.4*	−25.7 *−41.1*	2.3 *−14.9*	11.7 *−4.1*	12.8 *−2.9*	8.7 *−7.6*	10.0 *−8.1*	10.5 *−7.5*	23.6 *8.2*	13.9 *−3.4*
Average envelope RMS error [m s^{-2}]	0.0064 *0.0076*	0.0045 *0.0059*	0.0057 *0.0069*	0.0052 *0.0065*	0.0024 *0.0075*	0.0037 *0.0057*	0.0057 *0.0044*	0.0039 *0.0059*	0.0106 *0.0212*	0.0158 *0.0130*	0.0170 *0.0131*	0.0127 *0.0156*	0.0064 *0.0036*	0.0070 *0.0035*	0.0143 *0.0061*	0.0083 *0.0030*
Pearson's linear correlation coefficient	0.943 *0.938*	0.990 *0.985*	0.972 *0.964*	0.962 *0.955*	0.966 *0.953*	0.978 *0.972*	0.975 *0.967*	0.965 *0.953*	0.990 *0.988*	0.941 *0.937*	0.989 *0.988*	0.973 *0.971*	0.986 *0.989*	0.968 *0.974*	0.984 *0.987*	0.979 *0.984*

to a coefficient of determination (R^2) higher than 88 percent. The magnitudes of error in maximum acceleration amplitude for all tests in modes 2 and 3, averaging over all models with both methods of localisation of point of application of force, were found at 36.6 percent and 9.4 percent, respectively. The simulated responses might be affected by several error sources, such as uncertainties with the experimental dynamic model, unconsidered exogenous excitation sources, effects of human–structure interactions, errors in the reconstruction of magnitude and locations of GRF. These effects can cumulate or compensate each other. Broadly speaking, the results of simulations for mode 2 (T1 & T2) are worse than the results of simulations for mode 3 (T3 & T4). Mode 2 parameters were the more difficult to estimate experimentally, which might contribute to errors in the simulated responses for that mode. Nevertheless, the magnitudes of the estimated errors are remarkably good compared with the results of similar tests available in literature.

Previous work by Van Nimmen et al. [15] has found that pedestrian force models capturing the effect of variability in timing of the onset of pedestrian footsteps (see Section 1.2) outperform loading models based on an assumption of perfect periodicity. However, even with this allowance, the maximum simulated acceleration amplitude of the tested footbridge in the first vertical mode has been shown to overestimate the measured response twofold (equating to 200 percent error; cf. Fig. 18(b) in [15]). However, when comparing the results of this paper with those of [15] certain factors must be borne in mind. For example, differences in experimental conditions, i.e. properties of the tested bridges and experimental protocols – in particular excitation of the first vertical mode at 2.99 Hz by the second harmonic of force from four pedestrians in [14], and modelling, i.e. FEM in [15] and equivalent modal model herein. Previous work by Dang and Živanović [17] has found that the percentage difference in the average peak per cycle acceleration value of the structural response simulated based on force reconstructed from 19 MCS markers model, relative to the measured value, was within ± 20 percent at 92 percent confidence level. However, the movement of a load along the structure was not considered therein since the pedestrian was walking on a treadmill placed at the midspan of a composite bridge.

It is reported in [46] that walking over a surface with negative gradient results in reduction in step length, which is consistent with data presented in Fig. 21. This effect is not visible in Fig. 22, presenting data from tests in which the subject walked with pacing frequency of 2 Hz. It seems this effect is particularly strong for pacing frequencies lower than those preferred for normal walking. Nevertheless, considering data in Table 4, the slope of the walking surface does not seem to have a clear influence on the results.

The main advancement of the current loading model is that the pedestrian force is obtained directly from the motion of a single AHRS attached to a pedestrian. Although the force reconstruction gives better results than any other model presented so far, errors in the amplitude of force can still be expected. Nevertheless, it has been shown in Section 2.4.1 that the temporal congruence of the reconstructed and directly measured force is very good. Indeed, this might be the reason the proposed loading model performs so well. The main source of discrepancy in simulated response amplitudes in [15] was assigned to human–structure interaction, in particular additional damping from walking pedestrians unaccounted for in the adopted loading model of [16]. It was shown that better accuracy of the simulated response amplitudes could be obtained by increasing damping ratio of the considered vertical mode from 0.19 percent to 0.8 percent, which corresponds to 0.15 percent increase in damping ratio per pedestrian. Less accurate results were obtained by running the simulations based on this assumption for all tests in the current study presented in Section 5.1. Considering relatively low measured damping of mode 2 and 3 (see Table 3) there is some indirect evidence that, if the effect of additional damping is persistent, it is captured by the loading model. However, further work is necessary to gain confidence in this feature of the model.

Applying the oGRF reconstruction algorithm on average improved the magnitude of error in maximum amplitude of response for tests at mode 3 by 140 percent (see Section 5.1.2), but detrimental results were obtain for mode 2, for which the magnitude of error increased by 43 percent (see Section 5.1.1). Taking into account the results in Table 4 it may appear this step of the framework does not significantly (or in an obvious way) affect the results for the tests presented herein, but certain aspects of the experimental campaign need to be borne in mind in this assessment. Specifically, the pacing frequency of the pedestrian was enforced with a metronome providing strong stimulus for gait rhythmicity. This in turn can cause the pedestrian velocity to be fairly constant, reducing the natural step-to-step variability in gate parameters captured by oGRF, which in turn reduces the difference between the results obtained by the two algorithms. Furthermore, because BB is relatively long and the considered mode shapes are of relatively low order (i.e. have few nodal points), the rate of change of the amplitude of modal force due to changing pedestrian location is generally slow and has relatively little influence on the response. For this reason it is expected that that the proposed procedure for reconstructing oGRF could bring considerable improvements of accuracy of the simulated response for shorter bridges.

When simulating the response of the bridge, the importance of accurate location tracking increases when oGRF is near a node. This is because the mode shape amplitude is almost null (near the node) but the rate of change of the modal amplitude is high. Therefore, in this region, small differences in location of the force can cause relatively high differences in the response calculated, i.e. the more nodal points the pedestrian crosses the more likely oGRF will give superior results. Another possible reason for the superior performance of the framework in mode 3 can be seen by examining modes 2 and 3 in Fig. 19. The amplitude of mode shape 2 for the Northern section changes relatively slowly going from North to South, whereas the amplitude of mode shape 3 changes relatively quickly for the full length of the bridge. Both of the above are potential reasons for the better performance of the framework for mode 3 tests compared to mode 2 tests.

The same effect can be expected for tests in which pedestrian speed varies due to effects other than natural step-to-step variability, e.g. for walking in a crowd in which pedestrian gait patterns might be affected by close proximity of others, thus the assumption of linear progression of point of application of force is no longer substantiated. Another benefit of using the

algorithm for reconstructing oGRF is when studying the behaviour of individual pedestrians within a crowd of walkers. This is because the knowledge of pedestrian location relative to the location of other pedestrians and the mode shape is prerequisite for unveiling potential interaction mechanisms between different elements of crowd–structure system.

There are a number of limitations in the application/execution of the proposed framework, which need to be pointed out. More advanced PDR algorithms than used in this study are currently available [38]. For example, some of these algorithms account for drift in magnetometer readings associated with interference from magnetic fields other than that of the Earth (e.g. conducting wires or ferromagnetic materials used in construction), which can reduce heading errors. Other algorithms make better allowance of rolling motion of the foot during transition from stance to swing phase of gait in recognition of stationary periods in foot motion. It is expected the accuracy of the results obtained with (approximate) oGRF could be improved by using these algorithms. Nevertheless, it has been shown in this study, for the first time in the field of research concerned with the dynamic stability of structures, that a set of two AHRS can be used to obtain reliable data on pedestrian force and point of application of that force in situ.

6. Conclusions

The ambition of this study is to contribute to the development of a new class of pedestrian loading models, calibrated based on data representative of real pedestrian behaviour on full-scale structures. In order to accomplish this goal, a framework for the determination of localised pedestrian forces has been developed which uses wireless altitude and heading reference systems (AHRS). Importantly, in contrast to other models of structural loading on full-scale structures, the current framework does not require any extrapolations as to the temporal characteristics and amplitudes of pedestrian force. The framework relies on two main tasks:

- identification of pedestrian vertical loading from a single point inertial measurement taken from a suitable body landmark;
- determination of the point of application of pedestrian force based on data from a monitor attached to one foot.

To formulate the pedestrian vertical load model a dedicated experimental campaign was conducted during which six subjects walked on an instrumented treadmill at six speeds ranging from slow to normal, while instrumented with AHRS attached at the sternum, navel, lower back and seventh cervical vertebra. It has been shown that the force model built based on data from seventh cervical vertebra was able to yield an absolute error in the amplitude of the component of force at the pacing frequency of less than 15 percent at 90 percent confidence level. This is better than any other loading model presented so far. Furthermore, very good temporal congruence of the data reconstructed from the model with the benchmark data from the instrumented treadmill has been found, giving some confidence in applicability of the model for analysis of interactions in crowd–structure system.

An algorithm for the determining the origin of ground reaction force vector has been developed which utilises pedestrian dead reckoning and accounts for the bipedal nature of human gait. A single AHRS attached to one foot has been shown to be enough to accomplish this task for pedestrians walking on a footbridge which has one dominant direction of travel.

To validate the proposed modelling framework a dedicated experimental campaign was conducted on a full scale outdoor footbridge during which a pedestrian walked at frequencies of two vertical modes. Remarkably good match between the measured and simulated response of the bridge was found for both modes, accounting for the effect of the slope of the walking surface.

The developed framework allows the information of the behaviour of all components of crowd–structure system to be gathered thus allowing any emergent phenomena to be identified. Specifically, human-to-structure and human-to-human interactions are the core mechanisms assumed in many models of crowd behaviour and the associated structural loading to contribute to structural instability. These mechanisms have so far escaped rigorous empirical verification. The developed framework could facilitate this process.

Acknowledgements

The research presented here was funded by EPSRC (Grant EP/I029567/2). Authors thank Devon County Council for permitting the experimental campaign to be conducted on Baker Bridge in Exeter, UK, and Dr. Erfan Shahabpour (supported by EPSRC Grant EP/K03877X/1) for providing access to and assisting with measurements on the ADAL-3D treadmill at the University of Sheffield (funded by EPSRC Grant EP/E018734/1).

References

[1] J.H.G. Macdonald, Lateral excitation of bridges by balancing pedestrians, *Proceedings of the Royal Society A: Mathematical, Physical and Engineering Science* 465 (2009) 1055–1073, http://dx.doi.org/10.1098/rspa.2008.0367.

[2] M. Bocian, J.H.G. Macdonald, J.F. Burn, Biomechanically inspired modelling of pedestrian-induced forces on laterally oscillating structures, *Journal of Sound and Vibration* 331 (2012) 3914–3929, http://dx.doi.org/10.1016/j.jsv.2012.03.023.

[3] M. Bocian, J.H.G. Macdonald, J.F. Burn, Biomechanically inspired modeling of pedestrian-induced vertical self-excited forces, *Journal of Bridge Engineering* 18 (2013) 1336–1346, http://dx.doi.org/10.1061/(ASCE)BE.1943-5592.0000490.

[4] A. McRobie, G. Morgenthal, D. Abrams, J. Prendergast, Parallels between wind and crowd loading of bridges, *Philosophical transactions. Series A, Mathematical, Physical and Engineering Sciences* 371 (2013) 20120430, http://dx.doi.org/10.1098/rsta.2012.0430.

[5] M. Bocian, J.H.G. Macdonald, J.F. Burn, Probabilistic criteria for lateral dynamic stability of bridges under crowd loading, *Computers & Structures* 136 (2014) 108–119, http://dx.doi.org/10.1016/j.compstruc.2014.02.003.

[6] E.T. Ingólfsson, C.T. Georgakis, F. Ricciardelli, J. Jönsson, Experimental identification of pedestrian-induced lateral forces on footbridges, *Journal of Sound and Vibration* (2011) 1265–1284, http://dx.doi.org/10.1016/j.jsv.2010.09.034.

[7] S.P. Carroll, J.S. Owen, M.F.M. Hussein, Experimental identification of the lateral human–structure interaction mechanism and assessment of the inverted-pendulum biomechanical model, *Journal of Sound and Vibration* 333 (2014) 5865–5884, http://dx.doi.org/10.1016/j.jsv.2014.06.022.

[8] M. Bocian, J.H.G. Macdonald, J.F. Burn, D. Redmill, Experimental identification of the behaviour of and lateral forces from freely-walking pedestrians on laterally oscillating structures in a virtual reality environment, *Engineering Structures* 105 (2015) 62–76, http://dx.doi.org/10.1016/j.engstruct.2015.09.043.

[9] M. Bocian, *Determination of the self-excited forces on structures due to walking pedestrians using a biologically-inspired approach (Ph.D. thesis)*, University of Bristol, 2014.

[10] S.-H. Kim, K.-I. Cho, M.-S. Choi, J.-Y. Lim, Development of human body model for the dynamic analysis of footbridges under pedestrian induced excitation, *International Journal of Steel Structures* 8 (2008) 333–345.

[11] V. Racic, A. Pavic, J.M.W. Brownjohn, Experimental identification and analytical modelling of human walking forces: Literature review, *Journal of Sound and Vibration* 326 (2009) 1–49, http://dx.doi.org/10.1016/j.jsv.2009.04.020.

[12] E.T. Ingólfsson, C.T. Georgakis, J. Jönsson, Pedestrian-induced lateral vibrations of footbridges: A literature review, *Engineering Structures* 45 (2012) 21–52, http://dx.doi.org/10.1016/j.engstruct.2012.05.038.

[13] M. Haghighi, M. Bocian, O. Oddbjornsson, J.H.G. Macdonald, J.F. Burn, Synchronous data acquisition from large-scale clustered wireless sensor networks, *APWCS 2013 – 10th IEEE Vehicular Technology Society Asia Pacific Wireless Communications Symposium*, 22–23 August 2013, Seoul, Korea, 2013.

[14] P. Dallard, T. Fitzpatrick, A. Flint, A. Low, R. Ridsdill Smith, M.R. Willford, M. Roche, London Millenium Bridge: pedestrian-induced lateral vibration, *ASCE Journal of Bridge Engineering* 6 (2001) 412–417.

[15] K. Van Nimmen, G. Lombaert, I. Jonkers, G. De Roeck, P. Van den Broeck, Characterisation of walking loads by 3D inertial motion tracking, *Journal of Sound and Vibration* 333 (2014) 5212–5226, http://dx.doi.org/10.1016/j.jsv.2014.05.022.

[16] Q. Li, J. Fan, J. Nie, Q. Li, Y. Chen, Crowd-induced random vibration of footbridge and vibration control using multiple tuned mass dampers, *Journal of Sound and Vibration.* 329 (2010) 4068–4092, http://dx.doi.org/10.1016/j.jsv.2010.04.013.

[17] H.V. Dang, S. Živanović, Experimental characterisation of walking locomotion on rigid level surfaces using motion capture system, *Engineering Structures* 91 (2015) 141–154, http://dx.doi.org/10.1016/j.engstruct.2015.03.003.

[18] D.A. Winter, *Biomechanics and Motor Control of Human Movement*, 4th ed. John Wiley & Sons, Inc, Hoboken, USA, 1990.

[19] V. Racic, J.M.W. Brownjohn, A. Pavic, Reproduction and application of human bouncing and jumping forces from visual marker data, *Journal of Sound and Vibration* 329 (2010) 3397–3416, http://dx.doi.org/10.1016/j.jsv.2010.02.021.

[20] V. Racic, A. Pavic, J.M.W. Brownjohn, Modern facilities for experimental measurement of dynamic loads induced by humans: a literature review, *Shock and Vibration* 20 (2013) 53–67, http://dx.doi.org/10.3233/SAV-2012-0727.

[21] A. Pachi, T. Ji, Frequency and velocity of people walking, *Structural Engineering* 83 (2005) 36–40.

[22] Medical Developement, Analysis treadmil: ADAL 3D, ⟨http://www.medical-developpement.com/products/analysis-treadmill-adal-3d/⟩, 2015 (accessed 01.09.15).

[23] APDM, Inc., Wearable sensors: the Opal, ⟨http://www.apdm.com/wearable-sensors/⟩, 2014 (accessed 01.09.14).

[24] Codamotion, ⟨http://www.codamotion.com/⟩, 2014 (accessed 01.09.14).

[25] S.O.H. Madgwick, A.J.L. Harrison, R. Vaidyanathan, Estimation of IMU and MARG orientation using a gradient descent algorithm, *Proceedings of the IEEE International Conference on Rehabilitation Robotics*, 2011. doi:10.1109/ICORR.2011.5975346.

[26] S.P. Carroll, J.S. Owen, M.F.M. Hussein, Reproduction of lateral ground reaction forces from visual marker data and analysis of balance response while walking on a laterally oscillating deck, *Engineering Structures* 49 (2013) 1034–1049, http://dx.doi.org/10.1016/j.engstruct.2012.12.028.

[27] M.G. McDonald, S. Živanović, Measuring dynamic force of a jumping person by monitoring their body kinematics, *RASD 2013 – 11th International Conference on Recent Advances in Structural Dynamics*, Pisa, Italy, 2013.

[28] L. Tesio, V. Rota, C. Chessa, L. Perucca, The 3D path of body centre of mass during adult human walking on force treadmill, *Journal of Biomechanics* 43 (2010) 938–944, http://dx.doi.org/10.1016/j.jbiomech.2009.10.049.

[29] J.B. Kuipers, *Quaternions and Rotation Sequences: A primer with Applications to Orbits, Aerospace, and Virtual Reality*, Princeton University Press, 2002.

[30] M.T. Taner, F. Koehler, Velocity spectra – digital computer derivation and applications of velocity functions, *Geophysics* 34 (1969) 859, http://dx.doi.org/10.1190/1.1440058.

[31] National Health Service (NHS), Health Survey for England – 2013 Trend Tables, London, UK, 2013.

[32] J.E. Bertram, A. Ruina, Multiple walking speed–frequency relations are predicted by constrained optimization, *Journal of Theoretical Biology* 209 (2001) 445–453.

[33] M.H. Cole, W. Van Den Hoorn, J.K. Kavanagh, S. Morrison, P.W. Hodges, J.E. Smeathers, G.K. Kerr, Concurrent validity of accelerations measured using a tri-axial inertial measurement unit while walking on firm, compliant and uneven surfaces, *PLoS One.* 9 (2014) 1–12, http://dx.doi.org/10.1371/journal.pone.0098395.

[34] Y. Fujino, B.M. Pacheo, S.-I. Nakamura, P. Warnitchai, Synchronisation of human walking observed during lateral vibration of a congested pedestrian bridge, *Earthquake Engineering & Structural Dynamics* 22 (1993) 741–758.

[35] S. Nakamura, Field measurements of lateral vibration on a pedestrian suspension bridge, *Structural Engineering* 81 (2003) 22–26.

[36] J. Yoshida, Y. Fujino, Y. Sugiyama, T. Image, processing for capturing motions of crowd and its application to pedestrian-induced lateral vibration of a footbridge, *Shock and Vibration* 14 (2007) 251–260.

[37] M.C. Araújo Jr, H.M.B.F. Brito, R.L. Pimentel, Experimental evaluation of synchronisation in footbridges due to crowd density, *Structural Engineering International* 19 (2009) 298–303, http://dx.doi.org/10.2749/101686609788957784.

[38] R. Harle, A Survey of indoor inertial positioning systems for pedestrians, *IEEE Communications Surveys & Tutorials* 15 (2013) 1281–1293.

[39] X.Y.X. Yun, E.R. Bachmann, H. Moore, J. Calusdian, Self-contained position tracking of human movement using small inertial/magnetic sensor modules, *Proceedings 2007 IEEE International Conference on Robotics and Automation*, 2007. doi:10.1109/ROBOT.2007.363845.

[40] E. Foxlin, Pedestrian tracking with shoe-mounted inertial sensors, *IEEE Computer Graphics and Applications* 25 (2005) 38–46, http://dx.doi.org/10.1109/MCG.2005.140.

[41] J.M.W. Brownjohn, F. Magalhães, E. Caetano, A. Cunha, Ambient vibration re-testing and operational modal analysis of the Humber Bridge, *Engineering Structures* 32 (2010) 2003–2018.

[42] J.M.W. Brownjohn, P. Reynolds, S.K. Au, D. Hester, M. Bocian, Experimental modal analysis of civil structures: state of the art, *Proceedings of the 7th International Conference on Structural Health Monitoring of Intelligent Infrastructure*, Turin, Italy, 2015.
[43] D.J. Ewins, *Modal testing: theory, practice and application*, 2nd ed. Research Studies Press, Ltd., Baldock, England, 2000.
[44] H. Bachmann, A.J. Pretlove, J.H. Rayner, Vibrations induced by people, in: Vibration problems in structures: practical guidelines, 1995, pp. 1–28. doi:10.1007/978-3-0348-9231-5.
[45] BSI, BS EN 1991-1−2 Eurocode 1. Actions on structures – Part 2: Traffic loads on bridges, British Standards Institution, 2003.
[46] J. Sun, M. Walters, N. Svenson, D. Lloyd, The influence of surface slope on human gait characteristics: a study of urban pedestrians walking on an inclined surface, *Ergonomics.* 39 (1996) 677–692, http://dx.doi.org/10.1080/00140139608964489.